



**HAL**  
open science

## Stable isotopes in surface waters of the Atlantic Ocean: Indicators of ocean-atmosphere water fluxes and oceanic mixing processes

Marion Benetti, Gilles Reverdin, Giovanni Aloisi, Árný Erla Sveinbjörnsdóttir

► **To cite this version:**

Marion Benetti, Gilles Reverdin, Giovanni Aloisi, Árný Erla Sveinbjörnsdóttir. Stable isotopes in surface waters of the Atlantic Ocean: Indicators of ocean-atmosphere water fluxes and oceanic mixing processes. *Journal of Geophysical Research. Oceans*, 2017, 122 (6), pp.4723 - 4742. 10.1002/2017JC012712 . hal-01685203

**HAL Id: hal-01685203**

**<https://hal.science/hal-01685203>**

Submitted on 4 Jan 2022

**HAL** is a multi-disciplinary open access archive for the deposit and dissemination of scientific research documents, whether they are published or not. The documents may come from teaching and research institutions in France or abroad, or from public or private research centers.

L'archive ouverte pluridisciplinaire **HAL**, est destinée au dépôt et à la diffusion de documents scientifiques de niveau recherche, publiés ou non, émanant des établissements d'enseignement et de recherche français ou étrangers, des laboratoires publics ou privés.

Copyright

## RESEARCH ARTICLE

10.1002/2017JC012712

## Key Points:

- The distinct regional  $S$ - $\delta$  distributions are used to identify different surface water masses and their horizontal advection
- The surface  $\delta$ - $S$  distribution is used to indicate the relative importance of evaporation and meteoric water inputs
- We interpret the seawater  $\delta^{18}\text{O}$ - $\delta\text{D}$  distribution considering the kinetic fractionation processes associated to atmospheric water cycle

## Correspondence to:

M. Benetti,  
marioncb@hi.is

## Citation:

Benetti, M., G. Reverdin, G. Aloisi, and Á. Sveinbjörnsdóttir (2017), Stable isotopes in surface waters of the Atlantic Ocean: Indicators of ocean-atmosphere water fluxes and oceanic mixing processes, *J. Geophys. Res. Oceans*, 122, 4723–4742, doi:10.1002/2017JC012712.

Received 18 JAN 2017

Accepted 17 APR 2017

Accepted article online 24 APR 2017

Published online 10 JUN 2017

## Stable isotopes in surface waters of the Atlantic Ocean: Indicators of ocean-atmosphere water fluxes and oceanic mixing processes

M. Benetti<sup>1,2</sup> , G. Reverdin<sup>2</sup>, G. Aloisi<sup>2</sup>, and Á. Sveinbjörnsdóttir<sup>1</sup>

<sup>1</sup>Institute of Earth Sciences, University of Iceland, Reykjavik, Iceland, <sup>2</sup>LOCEAN, Sorbonne Universités, UPMC/CNRS/IRD/MNHN, Paris, France

**Abstract** The surface ocean hydrological cycle is explored based on  $\sim 300$  new  $\delta^{18}\text{O}$  and  $\delta\text{D}$  measurements from surface waters of the Atlantic Ocean and the Mediterranean Sea over the period 2010–2016. Our approach combines these surface observations with salinity ( $S$ ) and stable isotope measurements of atmospheric water vapor. The distinct regional  $S$ - $\delta$  distributions are used to identify different surface water masses and their horizontal advection. Moreover, based on assumptions on the  $\delta$ - $S$  characteristics of seawater sources and the isotope composition of the evaporative ( $\delta_e$ ) and meteoric water ( $\delta_{\text{MW}}$ ) fluxes, the  $\delta$ - $S$  distribution is used to indicate the relative importance of evaporation ( $E$ ) and meteoric water inputs ( $MW$ ). Here  $\delta_e$  is estimated from the Craig and Gordon's equation using 120 days of measurements of the ambient air above the Atlantic Ocean collected during three cruises. To provide quantitative estimates of the  $E$ : $MW$  ratio, we use the box model from Craig and Gordon (1965). This identifies the subtropical gyre as a region where  $E$ : $MW \sim 2$  and the tropical ocean as a region where  $MW$ : $E \sim 2$ . Finally, we show that the  $\delta^{18}\text{O}$ - $\delta\text{D}$  distribution is better represented by a linear fit than the  $\delta$ - $S$  relationship, even in basins governed by different hydrological processes. We interpret the  $\delta^{18}\text{O}$ - $\delta\text{D}$  distribution considering the kinetic fractionation processes associated with evaporation. In the tropical region where  $MW$  exceeds  $E$ , the  $\delta^{18}\text{O}$ - $\delta\text{D}$  distribution identifies the  $MW$  inputs from their kinetic signature, whereas in regions where  $E$  exceeds  $MW$ , the  $\delta^{18}\text{O}$ - $\delta\text{D}$  distribution traces the humidity at the sea surface.

### 1. Introduction

Significant changes in the global water cycle are expected as a result of the ongoing global warming of the earth surface. In particular, the modification of evaporation ( $E$ ) and precipitation ( $P$ ) will impact surface ocean salinity, and thus upper ocean stratification, with strong implications for primary production and carbon transfer [e.g., Schmitt, 1995; Terray *et al.*, 2012; Durack, 2015]. Studies have already documented an increase of the evaporation rate in the North Atlantic subtropical gyre since the 1970s [Yu, 2007] and a recent increase in the amount of precipitation in the Arctic region [e.g., Peterson *et al.*, 2002; Bintanja and Selten, 2014]. These observations portend future climate change with an amplified water cycle [Durack *et al.*, 2013]. Nevertheless, uncertainties on these estimations are large due to the difficulty to directly measure  $E$  and  $P$  over a sufficiently large spatial and temporal coverage. In order to accurately project future changes in the atmospheric hydrological cycle, we need to improve our knowledge of the spatial variability and controls on  $E$ - $P$  fluxes over the modern ocean.

The stable isotopic composition of surface seawater, combined with its salinity, is an effective tool to investigate hydrological processes at the surface of the ocean. Indeed, the relationship between these parameters is most of the time linear at the regional scale, with a slope and intercept that vary according to the hydrological conditions as different water sources and sinks have distinct isotopic compositions [Craig and Gordon, 1965]. Isotope fractionation during phase changes results in a general decrease of both  $\delta^{18}\text{O}$  and  $\delta\text{D}$  of water vapor and precipitation with increasing latitudes or altitude [Dansgaard, 1954]. The influence of water fluxes ( $E$  and meteoric water ( $MW$ ), corresponding to precipitation over the ocean plus river inputs) on the  $\delta$ - $S$  relationship at the ocean surface is illustrated in Figure 1. When a surface ocean water mass is diluted with  $MW$ , the  $Y$  intercept of the  $S$ - $\delta$  relationship represents the isotopic composition of the freshwater source ( $\delta_{\text{MW}}$ ). If, instead, the freshwater fluxes are dominated by evaporation, the  $Y$  intercept theoretically approaches the isotope

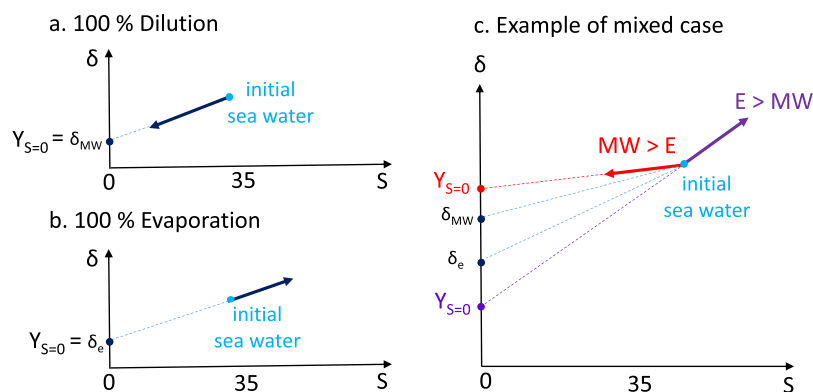


**Figure 1.** Control of evaporation (E) and meteoric water (MW) fluxes on the surface  $\delta$ -S relationship. (a) The salinity decreases according to dilution with MW and the Y intercept ( $Y_{S=0}$ ) indicates the  $\delta$  value of the MW. (b) The salinity increases according to E and the  $Y_{S=0}$  indicates the  $\delta$  value of the evaporated flux. (c) Mixed case where E and MW affect together the system and  $\delta_{MW} > \delta_e$ . If  $E > MW$ , the  $Y_{S=0}$  will be lower than  $\delta_e$ . If  $MW > E$ , the  $Y_{S=0}$  will be higher than  $\delta_{MW}$ .

composition of the evaporative flux ( $\delta_e$ ) [Craig and Gordon, 1965]. In practice, however, the oceanic surface S- $\delta$  relationship is affected by mixing in different proportions of multiple moisture end-members such as evaporation, MW inputs, and oceanic water masses, leading to Y intercept values that are not easy to interpret (see one example in Figure 1c where MW and E influence the water masse).

As a result, there is a strong diversity in the  $\delta$ -S relationship of the different regions of the global ocean [e.g., Rohling and Bigg, 1998; Schmidt, 1999; Benway and Mix, 2004; LeGrande and Schmidt, 2006]. This diversity is controlled by mixing between end-member water masses and by other surface hydrological processes such as evaporation, precipitation, runoff, sea ice processes, and continental glacial melt [e.g., Craig and Gordon, 1965; Rohling and Bigg, 1998; Benetti et al., 2016, 2017a; Benway and Mix, 2004; LeGrande and Schmidt, 2006; Dodd et al., 2009; Delaygue et al., 2001; Sutherland et al., 2009]. The  $\delta^{18}\text{O}$ - $\delta\text{D}$  relationship can also be measured in seawater [Rohling, 2007; Schmidt et al., 1999] and carries information on kinetic isotope effects associated with evaporation [Craig, 1961; Dansgaard, 1964].

In this paper, we present the S- $\delta^{18}\text{O}$ , S- $\delta\text{D}$ , and  $\delta^{18}\text{O}$ - $\delta\text{D}$  surface relationships of the Atlantic Ocean and Mediterranean Sea to investigate the processes that drive the hydrological cycle at the sea surface south of  $55^\circ\text{N}$  (and excluding the western subpolar gyre). Approximately 300 seawater samples have been analyzed with a rigorous analytical method, resulting in a nearly homogeneous accuracy throughout the data set.  $\delta\text{D}$  measurements are less numerous than  $\delta^{18}\text{O}$  measurements in public databases such as Global Seawater Oxygen-18 Database of Schmidt et al. [1999]. To fill this data gap, this study mostly used the recent Cavity Ring Down Spectrometer technology [Crosson et al., 2002], which allows simultaneous measurements of both isotopes. The large spatial coverage records a diversity of hydrological regimes at the Atlantic Ocean surface. In addition, a dozen samples are from the northwestern Mediterranean Sea, a semienclosed basin where evaporation largely dominates the water budget. In order to estimate the isotopic composition of the evaporated flux [Craig and Gordon, 1965; Merlivat and Jouzel, 1979], we complement this data set with the continuous measurement of the isotopic composition of the water vapor and standard meteorological parameters above the Atlantic Ocean during several months over the period 2012–2015 [Benetti et al., 2017b].

## 2. Method

### 2.1. Sampling Area

This data set includes measurements of  $\delta^{18}\text{O}$ ,  $\delta\text{D}$ , and salinity in the surface Atlantic Ocean from  $-20^\circ\text{S}$  to  $55^\circ\text{N}$  carried out during several cruises in the period 2010–2016 (Figure 2). It also includes samples in the western part of the Mediterranean Sea in 2016. The cruises are listed in Table 1.

### 2.2. Measurements

The stable isotope ratio is expressed in delta notation ( $\delta^{18}\text{O}$  for oxygen 18 and  $\delta\text{D}$  for deuterium) defined as the per mil deviation of the  $^{18}\text{O}/^{16}\text{O}$  and  $\text{D}/\text{H}$  ratios in the seawater from the ratio in the Vienna Standard Mean Ocean Water (VSMOW). For example, the deuterium isotopic composition is expressed as,

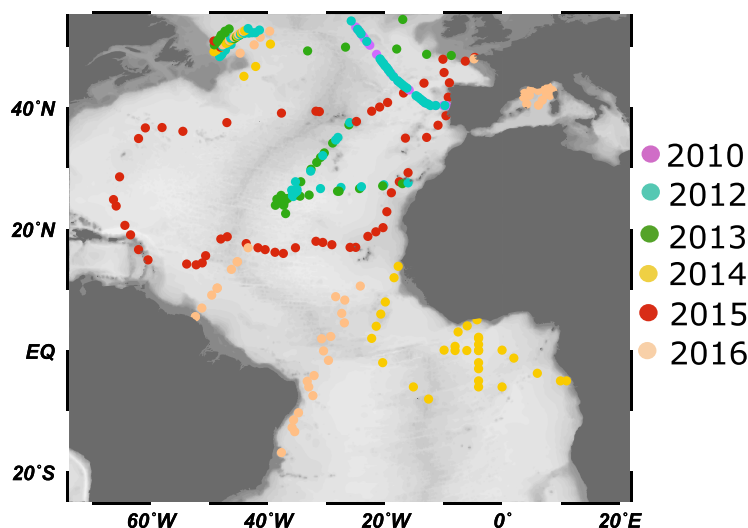


**Figure 2.** Sampling map for seawater  $\delta^{18}\text{O}$ ,  $\delta\text{D}$ , and surface salinity measurements from 2010 to 2016. The year of sampling is indicated by the color. Note that OVIDE 2010 in purple is below OVIDE 2012 in green (same transect from Lisbon to 55°N). The Newfoundland region has been sampled every 3 months from 2012 to 2016.

$$\delta\text{D} = \frac{R_{\text{sample}} - R_{\text{VSMOW}}}{R_{\text{VSMOW}}} \times 1000. \tag{1}$$

with  $R$  the ratio of concentrations of the heavy isotope to the light isotope (D/H), in the sample or in the international standard VSMOW.

The ~300 seawater samples of this study are collected either from the onboard thermosalinograph, or using a bottle rosette equipped with Niskin bottles. Then, samples were stored in 30 mL tinted glass bottles (GRAVIS). 289 samples have been analyzed with a PICARRO CRDS (cavity ring-down spectrometer; model L2130-I Isotopic H<sub>2</sub>O) at LOCEAN-IPSL (Paris, France). The remaining seawater samples have been measured with an Isotope Ratio Mass Spectrometer (Delta V Advantage IRMS coupled with a Gasbench II) at Institute of Earth Sciences (Reykjavik, Iceland). The four internal references which have been used to calibrate the data in the V-SMOW scale are  $\delta^{18}\text{O}$ : 0.51, -0.05, -3.26, and -6.61‰, and  $\delta\text{D}$ : 1.85, 0.46, -21.32, and -44.3‰. All reference waters, previously calibrated using IAEA references, are stored in steel bottles with a

**Table 1.** Main Characteristics of the Sampling Cruises<sup>a</sup>

Cruise	Region of Interest	Year	Ship	Method
PIRATA FR 24	Guinea Gulf	Apr–May 2014	RV Le Suroit (GENAVIR)	PICARRO L2130i after distillation
STRASSE	Eastern subtropical gyre	Aug–Sep 2012	RV La Thalassa (GENAVIR)	PICARRO L2130i after distillation
MIDAS	Eastern subtropical gyre	Mar 2013	RV Sarmiento de Gamboa (CSIC)	PICARRO L2130i after distillation
RARA	Brest-Cabo Verde-Martinique-Bermuda-Azores	Jan–Mar 2015 May–Jun 2015	RARA AVIS (AJD)	PICARRO L2130i after distillation
Fleur Australe	Eastern Atlantic 50°N	Feb 2016	Fleur Australe (P. Poupon)	PICARRO L2130i with liner
OVIDE 2010	Portugal – 55°N	Jun 2010	RV La Thalassa (GENAVIR)	PICARRO L2130i after distillation
OVIDE 2012	Portugal – 55°N	Jun–Jul 2012	RV Sarmiento de Gamboa	PICARRO L2130i after distillation
MOOSE-GE 2016	Mediterranean Sea	May–Jun 2016	RV Atalante (GENAVIR)	PICARRO L2130i with liner
TARA	Eastern Atlantic at 50°N	May and Dec 2013	Tara (Tara Expeditions)	PICARRO L2130i after distillation
SURATLANT	Southwestern subpolar gyre	2012–2016 (every 3 months)	EIMSKIP vessels	PICARRO L2130i Distillation or liner
Toucan/ Cap SanLorenzo/ Colibri	Equatorial Atlantic	Summer 2016	Toucan/Colibri (Maritime Nantaise) Cap San Lorenzo (Hamburg Sud)	PICARRO L2130i with liner or IRMS

<sup>a</sup>The method of measurement is indicated in the last column. Distillation and liner refer to modes of operation on the Picarro L2130i, whereas IRMS indicates that an isotope ratio mass spectrometer was used (see text for further information).

**Table 2.** Correction Applied to the 300 Isotopic Measurements Presented in This Study in Order to Report Isotopic Compositions on the Concentration Scale (After Having Removed the Salt Effect)<sup>a</sup>

Method	$\delta^{18}\text{O}$	$\delta\text{D}$
Distillation + Picarro	+0.14‰	+0.57
Liner + Picarro	+0.09‰	+0.12‰
IRMS	+0.07‰	-1.17‰

<sup>a</sup>The corrections are derived from several measurements of a freshwater standard of known isotopic composition and an artificial seawater made from this reference.

slight overpressure of dry nitrogen to avoid evaporation processes and exchanges with ambient air humidity. Based on repeat analyses of an internal laboratory standard over several months, the reproducibility of the measurements is better than  $\pm 0.05\text{‰}$  for  $\delta^{18}\text{O}$  and  $\pm 0.50\text{‰}$  for  $\delta\text{D}$ . About 85% of the PICARRO measurements have been done after having distilled the seawater samples to avoid salt accumulation in the vaporizer [Skrzypek and Ford, 2014]. The remaining 15% have been done without distillation prior to the PICARRO analyses but with the use of a wire mesh inserted in the vaporizer inlet to trap about 80% of the seawater salt (the liner has

been provided by Dave Hodell, University of Cambridge). For IRMS measurements, we follow the approach of Epstein and Mayeda [1953], in which measurements are obtained by equilibration between the reference gas and the liquid seawater sample. The presence of salts in liquid samples at seawater concentration (salinity  $\sim 35$ ) affects the IRMS and PICARRO measurements [e.g., Sofer and Gat, 1972, 1975; Bourg et al., 2001; Lécluyer et al., 2009; Skrzypek and Ford, 2014]. To check the consistency of the three different methods we used, the salt effect on the measurements was evaluated for each protocol. For this purpose, we prepared artificial seawater from a freshwater standard of known isotopic composition. The isotopic composition of the artificial seawater was measured by the three methods and corrections were derived to remove the salt effect on measurements of seawater for each of the three methods in question (Table 2). Notice that the salt effect corrections have been evaluated for the specific protocols of this study and might be different in other laboratories. Here we applied these corrections on the  $\sim 300$  samples of this study to obtain a consistent isotopic data set on the concentration scale [Sofer and Gat, 1972, 1975].

The salinity has been measured using a salinity probe, installed on a thermosalinograph or a CTD rosette, calibrated before and after each cruise. Additionally, measurements were calibrated with salinity samples analyzed on salinometers referenced to Standard Sea Water. SSS accuracies were generally estimated at 0.01 during the cruises. We express  $S$  in the practical salinity scale of 1978, pss-78, with no unit.

Moreover, 39 sea-rain samples from eight rain events have been collected in the Guinea Gulf during the PIRATA FR24 cruise. We used a simple manual rainwater trap top with narrow-mouthed funnel, located on the bridge. The isotope composition of these freshwater samples has been measured at LOCEAN with the same PICARRO used for the seawater measurements (no corrections applied on freshwater measurements).

### 3. The Study Area: Surface Hydrology and Water Masses

In this section we summarize the general surface hydrology and oceanic circulation of the Atlantic Ocean's lower and middle latitudes. The schematic surface circulation is shown in Figure 3, as well as sea surface salinity [Gaillard, 2016]. The  $15^{\circ}\text{N}$ – $40^{\circ}\text{N}$  latitudes are dominated by an anticyclonic subtropical gyre (STG) formed by the Gulf Stream (GS), the North Atlantic Drift (NAD), the Canary Current (CC), and the North Equatorial Current (NEC). The Azores Current is an extension of the GS, south of the NAD, and participates to the transport from the fresher outer STG to the more saline inner STG. The Labrador Current carries cold and freshwaters from the highest latitudes (mostly originating from the arctic region) and forms the western southward branch of the cyclonic subpolar gyre (SPG). The NAD is an extension of the GS diluted with fresher waters carried by the Labrador Current and constitutes the intergyre area (southern eastward branch of the SPG and northern eastward branch of the STG). Part of the NAD recirculates to the south across the CC. Then, the STG is bounded toward the South by the westward NEC. A similar STG is observed in the South Atlantic with anticyclonic gyre circulation. The South Equatorial Current (SEC) constitutes the northern branch of the southern Atlantic hemisphere STG and carries waters from the eastern to western part of the Atlantic. Part of it also flows northwestward along northern South America bringing this water to the northern hemisphere. The remaining part flows southward along the Brazil coast.

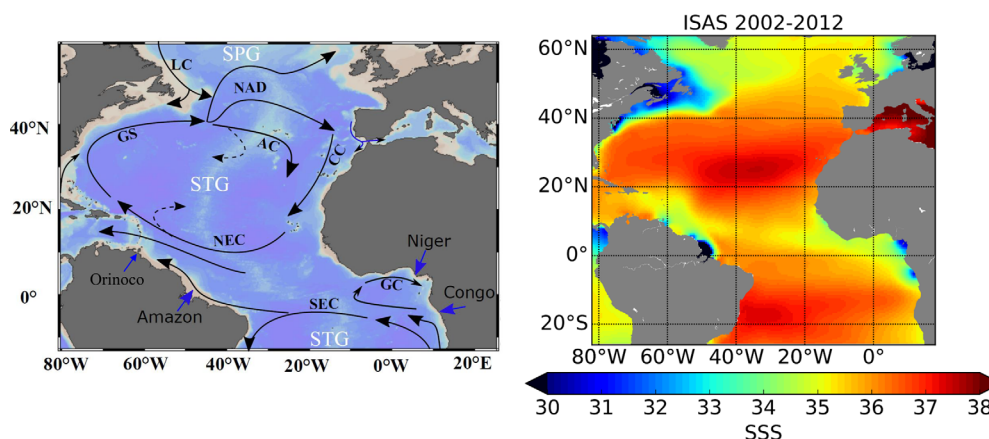


**Figure 3.** (left) Schematic surface circulation of the Atlantic Ocean from  $-15^{\circ}\text{S}$  to  $55^{\circ}\text{N}$ . STG and SPG are the subtropical and subpolar gyre, respectively. LC: Labrador Current, NAD: North Atlantic Drift, GS: Gulf Stream, AC: Azores Current, CC: Canary Current, NEC: North Equatorial Current, SEC: South Equatorial Current, GC: Guinea Current. The main estuaries in the tropics are indicated by the blue arrows (Amazon, Orinoco, Niger, and Congo rivers). The black dotted arrows represent the transport through eddies and Ekman transport from the outer to the inner North Atlantic STG. (right) Sea surface salinity annual average over the period 2002–2012. The data are from ISAS-13 (in situ analysis system) temperature and salinity gridded fields, SEANOE (sea open scientific data publication, [www.seanoe.org](http://www.seanoe.org)) [Gaillard, 2015].

The Atlantic Ocean's lower and middle latitudes can be divided into three main subareas governed by diverse hydrological regimes: (i) the temperate or midlatitude region, (ii) the tropical region, and (iii) the subtropical region. In addition, we also present (iv) the Mediterranean Sea as an example of a hydrologically restricted system subject to strong evaporation.

1. This study samples the temperate region in the eastern part of the Atlantic Ocean (east of  $30^{\circ}\text{W}$  and north of  $40^{\circ}\text{N}$ ), between the subtropical and polar region. This region forms the eastern and southern part of the SPG and is strongly influenced by waters carried along the NAD that contain a mixture between freshwaters from the Labrador Current and saltier waters from the GS. There the difference between the E and MW fluxes is less contrasted compared to the tropical and subtropical region, with probably similar magnitudes of E and MW fluxes (transition with the subtropical region where E exceeds MW and the northern latitudes where MW exceeds E) [Schmitt, 1995]. We also sample the southern and western part of the SPG, off Newfoundland (SURATLANT surveys), to identify the source of water from the SPG, that will be in part mixed with the GS to form the NAD.
2. The tropical region (Equator  $\pm 15^{\circ}$ ) is dominated by the input of MW in the form of precipitation over the ocean and river runoff along the African and South American coasts (see the lower salinity strip at  $\sim 5^{\circ}\text{N}$ – $10^{\circ}\text{N}$  in Figure 3). The locations of the three main estuaries are shown in Figure 3 (Niger, Congo, and Amazon) and are also identifiable by the three zones of freshwater along the coast (salinity below 31). In this tropical belt, the annual evaporation minus precipitation (E-P) is negative and mostly within the range  $-20$  to  $-125$  cm/yr [Schmitt, 1995]. The surface is also affected by deeper waters from the subtropical regions carried to the surface by the equatorial upwelling and other regional upwellings.
3. In the North Atlantic subtropical region (area characterized by high salinity around  $30^{\circ}\text{N}$ ), the annual E-P is positive and mainly comprised between 50 and 150 cm/yr, with the high values concentrated in the southeastern STG [Schmitt et al., 1989; Schmitt, 1995; Gordon and Giulivi, 2014]. The annual salinity maximum is identifiable in Figure 3 and is correlated with limited precipitation and a high evaporation rate a little further south [Wüst and Defant, 1936; Gordon and Giulivi, 2014; Durack, 2015]. The Gulf Stream area from  $30^{\circ}\text{N}$  to  $40^{\circ}\text{N}$  in the western part of the gyre is also probably dominated by evaporation but MW inputs are more abundant in this region, compared to the eastern part of the gyre. The positive E-P in the subtropics is compensated by convergence of freshwater through the Ekman transport and eddy fluxes, as well as the large-scale ocean advection from the North [Gordon and Giulivi, 2014].
4. The Mediterranean Sea is a semienclosed basin where fresh Atlantic waters enter at the surface across the Strait of Gibraltar. The strong E compared to MW inputs result in the transformation of Atlantic waters into saline Mediterranean Waters (salinity larger than 38). The salinity increases from the western part to the eastern part, where E is maximal with particularly dry continental air masses in contact with the ocean surface [Romanou et al., 2010]. Then, in specific areas in winter during strong dry wind events,

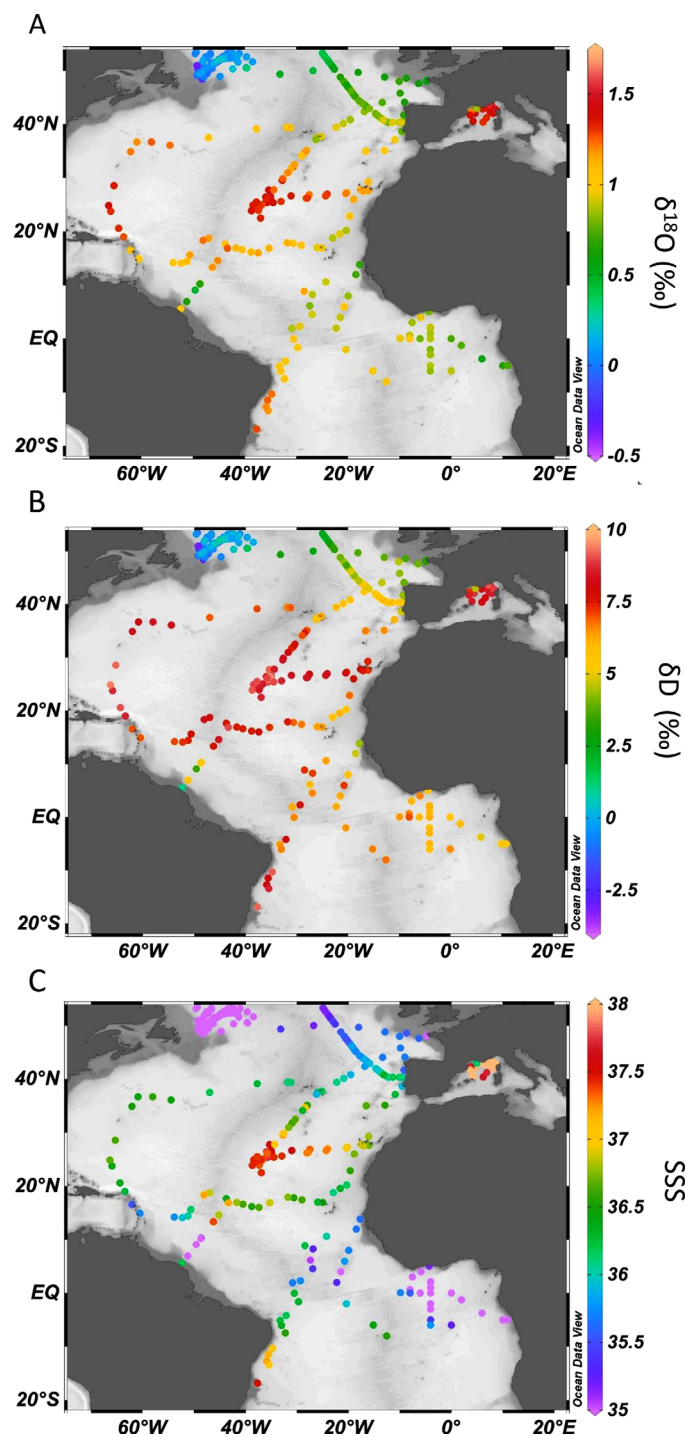


**Figure 4.** Spatial variability of the (a)  $\delta^{18}\text{O}$ , (b)  $\delta\text{D}$ , and (c) surface salinity with a color bar from 35 to 38 to better illustrate high-salinity variability.

$6^\circ\text{E}$ ,  $3.75^\circ\text{S}$ ). The lowest  $\delta$  values are found in the western part of the subpolar gyre (down to  $\delta^{18}\text{O} = -0.34\text{‰}$  and  $\delta\text{D} = -3.18\text{‰}$ ) with a corresponding salinity of 34.13.

#### 4.2. $\delta_e$ and $\delta_{MW}$

In order to later discuss the  $\delta$ -S relationships in the context of the regional water fluxes (E, MW, and the advective mixing processes), we first present the  $\delta_e$  and  $\delta_{MW}$  characteristics of the low and midlatitudes of the Atlantic Ocean.

surface waters become very dense and sink to form the intermediate (300–400 m) and deep (1000–3000 m) waters. These waters are then exported toward the Atlantic Ocean at depth across the Strait of Gibraltar. Remnants of this salty water mass can be identified at  $\sim 1000$  m depth over a large part of the North Atlantic basin [Bower et al., 2002].

## 4. Spatial Variability

### 4.1. $\delta^{18}\text{O}$ , $\delta\text{D}$ , and Salinity

The spatial variability of surface  $\delta^{18}\text{O}$ ,  $\delta\text{D}$ , and salinity is presented in Figure 4. The spatial coverage results in a large range for these quantities. Surface salinity varies from 30.48 to 38.35,  $\delta^{18}\text{O}$  from  $-0.34$  to  $1.48\text{‰}$ , and  $\delta\text{D}$  from  $-3.18$  to  $9.57\text{‰}$ . The high values of S and  $\delta$  correspond to regions of high evaporation. The heaviest isotopic compositions of the Atlantic Ocean ( $\delta^{18}\text{O} = 1.48\text{‰}$  and  $\delta\text{D} = 9.57\text{‰}$ ) were observed during the STRASSE summer cruise in the eastern part of the subtropical gyre, with a salinity of 37.76 (close to the maximal salinity of the STG, Figure 3). The highest surface salinities (up to 38.35) are found in the western Mediterranean Sea (the eastern Mediterranean Sea is not sampled). The lower S and  $\delta$  values indicate surface dilution with freshwater inputs. The lowest salinity (30.48) is found at  $52.37^\circ\text{W}/5.53^\circ\text{N}$ , over the Brazilian shelf strongly affected by freshwater input from the Amazon drainage area with a relatively high  $\delta$  values:  $\delta^{18}\text{O} = 0.14\text{‰}$  and  $\delta\text{D} = 1.02\text{‰}$ . Low salinities are also found in the Guinea Gulf, mainly in its eastern part (down to 32.55 at

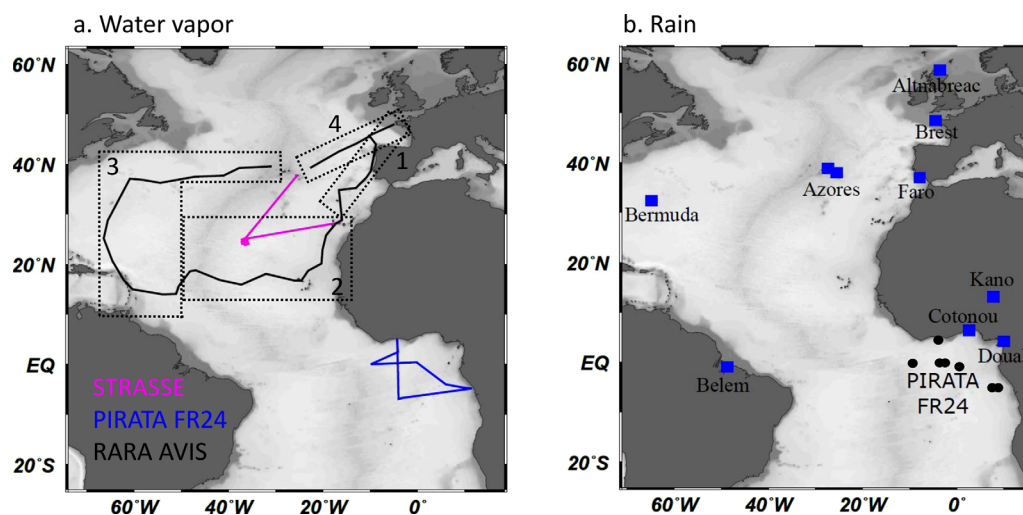


**Figure 5.** (a) Location of  $\delta^{18}\text{O}$  and  $\delta\text{D}$  measurements of the water vapor above the sea surface during the STRASSE, PIRATA FR24, and RARA cruise. The RARA cruise has been divided in four subsets according to the location and the season. (b) Location of  $\delta^{18}\text{O}$  and  $\delta\text{D}$  measurements of the rain. The blue squares are land GNIP stations and the black dots correspond to rainwater collection from the ship during the PIRATA FR24 cruise.

During the STRASSE, PIRATA, and RARA cruises, the standard meteorological parameters, as well as the isotopic composition of the water vapor have been continuously measured a few meters above the sea surface (see Figure 5a for sampling area). The measurements are fully described in *Benetti et al.* [2017b] and *Benetti et al.* [2014, 2015]. For all cruises, we calculate the average  $\delta_e$  weighted by the evaporation rate using the *Craig and Gordon's* [1965] equation (Table 3). The STRASSE cruise samples the eastern STG and the PIRATA cruise samples the Guinea Gulf. Because of the large spatial and temporal coverage, we divided the RARA cruise measurements in four subsets to calculate the average  $\delta_e$  values based on the location and the season. The four subsets are located in Figure 5a with the midlatitudes represented by subsets 1 and 4, the eastern part of the STG represented by subset 2, and the western part is represented by subset 3. The periods of measurement are described in Table 3.

For the six subsets, the weighted averages of  $\delta_e^{18}\text{O}$  and  $\delta_e\text{D}$  vary from  $-8.30$  to  $-4.94$ ‰ and from  $-54.06$  to  $-27.72$ ‰, respectively. The mean weighted  $\delta_e$  values are quite close for PIRATA and STRASSE cruises (in particular for  $^{18}\text{O}$ ), while PIRATA samples the Guinea Gulf in spring and STRASSE samples the eastern STG in summer. For the RARA cruise, the mean values are systematically lower for  $\delta_e^{18}\text{O}$  and  $\delta_e\text{D}$  (in particular for RARA 2, which is quite close to the site of the STRASSE cruise). The variability of the mean weighted  $\delta_e$  values results from the variability of surface conditions (humidity, SST, wind speed,  $\delta^{18}\text{O}$ , and  $\delta\text{D}$  in seawater and in the ambient air) in these regions [*Craig and Gordon*, 1965; *Merlivat and Jouzel*, 1979]. In particular, the difference between RARA 2 and STRASSE could be in part due to seasonal cycle in the eastern STG (RARA 2 was in winter, while STRASSE was in summer). Moreover, the midlatitude region has been sampled in winter (RARA I) and in summer (RARA IV) 2015: we found close  $\delta_e\text{D}$  values for both periods and a difference of about 1‰ between the two  $\delta_e^{18}\text{O}$  values. In the following interpretations, we only consider the measured variability of  $\delta_e^{18}\text{O}$  and  $\delta_e\text{D}$ , whereas what controls the  $\delta_e$  value is explored in a work in progress.

We then use the Global Network Isotopic Precipitation (GNIP) network to estimate the  $\delta_p$  spatial variability over the study area. The selected land stations are shown in Figure 5b and the subsequent annual average

**Table 3.** The Average of  $\delta_e$  for Each Cruise, Weighted by the Evaporation Rate<sup>a</sup>

Region	East STG		West STG	Guinea Gulf	Middle Latitudes	
Cruise	STRASSE	RARA 2	RARA 3	PIRATA	RARA 1	RARA 4
Duration (day)	24	17	27	22	14	11
Season	Summer 2012	Winter 2015	Winter and Summer 2015	Spring 2014	Winter 2015	Summer 2015
$\delta_e^{18}\text{O}$	-5.05	-8.30	-6.47	-4.94	-6.41	-5.42
$\delta_e\text{D}$	-31.02	-54.06	-48.15	-27.72	-48.68	-46.69

<sup>a</sup>The RARA cruise has been divided in four subsets according to the location and the season. We consider in the CG65 formula the smooth regime with  $\alpha_k = 1.006$  for  $\delta^{18}\text{O}$  and  $\alpha_k = 1.0035$  for  $\delta\text{D}$  [*Merlivat and Jouzel*, 1979] and the equilibrium fractionation factors from *Majoube* [1971].

**Table 4.** The Annual Average  $\delta_p$  Values Weighted by the Precipitation Rate From the 10 GNIP Stations From Figure 5b<sup>a</sup>

Location	$\delta_p^{18}\text{O}$ (‰)	$\delta_p\text{D}$ (‰)	d-excess (‰)
Brest (France)	$-5.26 \pm 0.52$	$-33.4 \pm 4.8$	$8.6 \pm 1.0$
Faro (Portugal)	$-4.52 \pm 0.74$	$-25.0 \pm 5.3$	$11.2 \pm 2.1$
Altrabreac (UK)	$-8.72 \pm 0.32$	$-59.3 \pm 3.3$	$10.5 \pm 0.7$
Douala (Cameroon)	$-3.07 \pm 0.69$	$-13.7 \pm 4.4$	$10.9 \pm 1.3$
Cotonou (Benin)	$-3.00 \pm 0.45$	$-12.6 \pm 3.3$	$11.5 \pm 0.3$
Kano (Niger)	$-4.28 \pm 1.81$	$-27.7 \pm 10.9$	$6.6 \pm 3.7$
Ponta Delgada (Azores)	$-3.97 \pm 0.90$	$-21.9 \pm 6.9$	$9.9 \pm 2.1$
Angra Do Heroismo (Azores)	$-3.86 \pm 0.68$	$-22.1 \pm 6.5$	$8.8 \pm 2.1$
Belem (Brazil)	$-2.62 \pm 1.44$	$-13.0 \pm 9.4$	$9.3 \pm 3.5$
Bermuda Island	$-3.49 \pm 0.35$	$-16.8 \pm 1.8$	$11.1 \pm 3.7$
Guinea Gulf (1–20 May 2014)	$-4.79 \pm 2.05$	$-27.0 \pm 16.4$	$11.4 \pm 2.9$

<sup>a</sup>The last row is the average value estimated from the 39 samples of rain collected during the PIRATA cruise (see Appendix A).

$\delta_p$  values weighted by the precipitation rate are presented in Table 4. Moreover, we also calculate the value of  $\delta_p$  in the Guinea Gulf from the 39 samples of rain collected during the PIRATA cruise during the period 1–20 May 2014 (see all values in Appendix A and averages in Table 4). The data record the meridional gradient with the most depleted  $\delta_p$  values observed at Altrabreac (UK) and the most enriched values at Belem (Brazil).

### 5. The $\delta^{18}\text{O}$ -S and $\delta\text{D}$ -S Relationships

The scatterplots in Figure 6 illustrate the variety of the surface S- $\delta^{18}\text{O}$  and S- $\delta\text{D}$  relationships in the Atlantic Ocean between 20°S and 55°N (see purple points, this study). At this large spatial scale, the 300 measurements do not fall on a single linear relationship, indicating that the Equatorial and North Atlantic Ocean are governed by a different surface hydrology. The highest salinities correspond to regions of strong evaporation such as the Mediterranean Sea and the STG, with a scatter in the S- $\delta$  distribution suggesting different

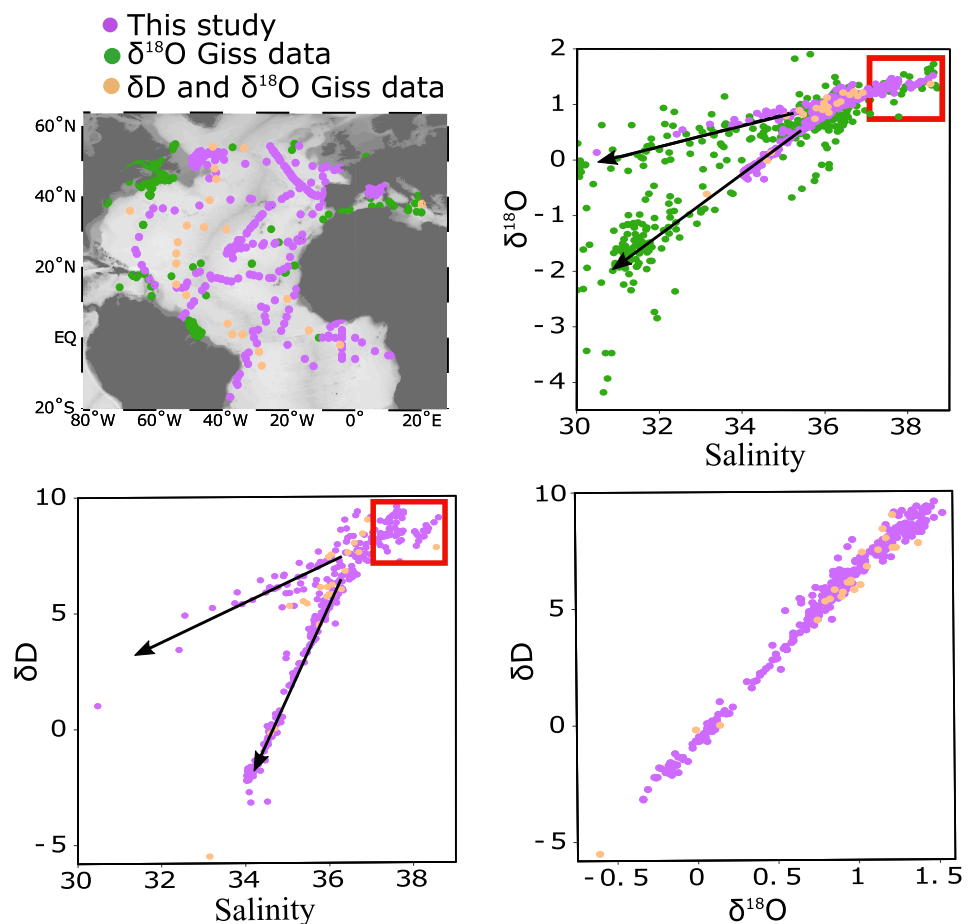


**Figure 6.** Comparison of  $\delta^{18}\text{O}$ -S,  $\delta\text{D}$ -S, and  $\delta^{18}\text{O}$ - $\delta\text{D}$  relationships from this study in purple (300 samples) with the GISS database (green and orange, 0–15 m and salinity more than 30). At this large scale, the various relationships reflect regions strongly affected by evaporation (E): (red square) as well as by dilution with meteoric water (MW): (black arrow).

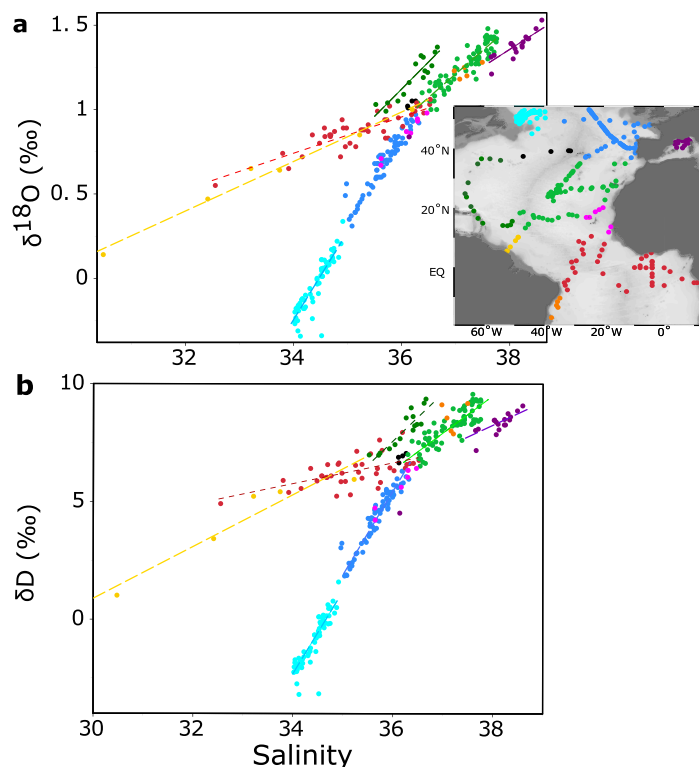


**Figure 7.** (a)  $\delta^{18}\text{O}$ -S and (b)  $\delta\text{D}$ -S scatterplots of the North Atlantic for different subgroups during the period 2010–2016. We do not calculate the linear regression for orange and black groups due to their small range of variation. The right figure provides the location of the samples in the different subgroups. Some samples are from the northwestern Mediterranean Sea (purple).

the region for samples with salinity larger than 30. Most of these samples are located over the continental shelf area (see green dots in Figure 6). Our new compilation of isotope values is a considerable improvement of the Atlantic Ocean surface spatial coverage and it is clear that the more limited GEOSECS  $\{\delta^{18}\text{O}-\delta\text{D}\}$  sampling does not record the complexity of the S- $\delta$  relationship over the Atlantic Ocean [Östlund *et al.*, 1987].

In the following, we highlight from this new data set distinct linear relationships from subareas to identify the different water masses affected by their own surface hydrological regimes. We group the data set into 10 different subgroups (we do not calculate the linear regression for two groups due to the small range of salinity variation). Figure 7 shows the different subgroups and their location (one color for a subgroup). The linear regressions for each group are presented in Table 5. In most of the subgroups, the correlation coefficient in these scatterplots is greater than 0.9.

### 5.1. The Midlatitudes

The midlatitudes from 38°N to 55°N correspond to intermediate salinity ranges (darker blue group in Figure 7). The salinity varies from 35.1 to 36.3,  $\delta^{18}\text{O}$  from 0.35 to 0.94‰, and  $\delta\text{D}$  from 1.85 to 6.30‰. The linear regressions are  $\delta^{18}\text{O} = 0.47 \cdot S - 16.06$  and  $\delta\text{D} = 3.39 \cdot S - 116.7$ . The Y intercept of the  $\delta$ -S relationships is not easy to interpret because this is a region where MW and E have similar magnitudes [Schmitt, 1995] and because average  $\delta_e$  and  $\delta_p$  are difficult to estimate with the advection processes carrying two contrasted water masses in the region. There is water from the lower latitudes carried by the NAD, with  $^{18}\text{O}$  and D-enriched freshwater inputs, and water from the southern part of the subpolar gyre carried by Ekman transport (eastward winds), with  $^{18}\text{O}$  and D-depleted freshwater inputs. Minor contribution of local river inputs around the Iberian Peninsula, France and UK is also expected. For these reasons, it is difficult to interpret the Y intercept value according to E, P,  $\delta_e$ , and  $\delta_p$  values. Therefore, our approach is to identify the main water masses affecting the system in the  $\delta$ -S

evaporation conditions (red square in Figure 6). The lowest salinity observed over the Brazilian shelf does not correspond to the lowest  $\delta$  values, which are found in the western part of the subpolar gyre (down to  $\delta^{18}\text{O} = -0.32$ ‰ and  $\delta\text{D} = -3.17$ ‰) with a corresponding salinity of 34.10. These saltier and more depleted samples, compared to those found in the Guinea Gulf or over the Brazilian shelf, reveal freshwater inputs from higher latitudes. This is an example of how dilution with different freshwater sources (the enriched tropical MW and the depleted high/middle latitudes MW) results in distinct  $\delta$ -S relationships (black arrows in Figure 6). Previously, only 24 surface  $\{\delta^{18}\text{O}-\delta\text{D}\}$  pair from the GEOSECS project were available for this region in the international Global Seawater Oxygen-18 Database of Schmidt *et al.* [1999]. Nevertheless,  $\delta^{18}\text{O}$  are more numerous than  $\delta\text{D}$  with 426 GISS measurements in

**Table 5.** Linear Regressions for  $\delta^{18}\text{O}$ -S,  $\delta\text{D}$ -S, and  $\delta^{18}\text{O}$ - $\delta\text{D}$  for the Eight Regions of Interest<sup>a</sup>

Region	S- $\delta^{18}\text{O}$	S- $\delta\text{D}$	$\delta^{18}\text{O}$ - $\delta\text{D}$	Comments and Cruises
Intergyre area (dark blue)	S = 0.47 Y = -16.06 R = 0.96 n = 67	S = 3.39 Y = -116.7 R = 0.95 n = 67	S = 7.09 Y = -0.66 R = 0.98 n = 67	Without two coastal samples on the shelf near Brest (influenced by local MW inputs) Cruises TARA 2013 (Dec and May) Ovide 2010 and 2012 (Jun/Jul) RARA 2015 (Jan and Jun) Fleur Australe (Feb 2016)
Eastern NASTG (light green)	S = 0.28 Y = -9.03 R = 0.92 n = 77	S = 1.58 Y = -50.57 R = 0.86 n = 77	S = 5.80 Y = +0.91 R = 0.95 n = 77	Cruises STRASSE 2012 (Aug/Sep) MIDAS 2013 (Mar) RARA 2015 (Feb)
Tropical Atlantic (red)	S = 0.11 Y = -3.04 R = 0.87 n = 41	S = 0.45 Y = -9.71 R = 0.60 n = 39	S = 4.73 Y = 2.16 R = 0.80 n = 39	Cruises PIRATAFR24 2014 (Apr/May) Cap San Lorenzo 2016 (Jul) Cap San Lorenzo 2016 (Aug)
Western NASTG (dark green)	S = 0.32 Y = -10.46 R = 0.92 n = 15	S = 2.04 Y = -65.80 R = 0.90 n = 15	S = 6.36 Y = 0.50 R = 0.99 n = 15	Cruises RARA 2015 (Mar and May) Colibri 2016 (Aug)
Med Sea (purple)	S = 0.21 Y = -6.48 R = 0.85 n = 16	S = 0.98 Y = -29.15 R = 0.76 n = 16	S = 5.07 Y = 1.37 R = 0.95 n = 16	Without the two freshest samples Including the two most saline samples (LIW at 370 m and bottom sample at 2600 m) Cruise MOOSE-GE 2016 (May/Jun)
Amazon Basin (yellow)	S = 0.15 Y = -4.29 R = 0.99 n = 6	S = 1.10 Y = -32.13 R = 0.95 n = 5	S = 7.44 Y = 0.12 R = 0.98 n = 5	Cruises Toucan 2016 (Aug) Colibri 2016 (Aug)
SW subpolar gyre (light blue)	S = 0.52 Y = -17.87 R = 0.95 n = 58	S = 3.51 Y = -121.60 R = 0.95 n = 58	S = 6.57 Y = -0.67 R = 0.97 n = 58	Without the three most depleted samples affected by brines during winter Cruise Suratlant 2012–2016 (every 3 months)
Upwelling influence (magenta)	S = 0.35 Y = -11.81 R = 0.99 n = 7	S = 2.39 Y = -80.70 R = 0.98 n = 7	S = 6.86 Y = -0.26 R = 0.98 n = 7	Cruises RARA 2015 (Feb) PIRATAFR24 2014 (May)

<sup>a</sup>The five samples around the Brazil current (orange group without linear regression) have been collected in July and August 2016 aboard TOUCAN. LIW: Levantine Intermediate Water. The color indicated in bracket corresponds to the color in Figure 7.

diagram. To identify the SPG source, we use the samples off the coast of Newfoundland with salinity between 34 and 35 (SURATLANT cruises over the 2010–2016 period, cyan group in Figure 7). The lower latitude sources carried by the NAD can be represented by the four samples (black group) with quite similar salinity (36) and isotopic composition ( $\sim 1\text{‰}$  for  $\delta^{18}\text{O}$  and  $\sim 7\text{‰}$  for  $\delta\text{D}$ ) located West of the Azores Islands, as well as two samples (light green) slightly north of Madeira Island with salinity about 36.5–36.6 and  $\delta^{18}\text{O} \sim 0.86\text{‰}$ ,  $\delta\text{D} \sim 6\text{‰}$ . Considering these end-members, the observed  $\delta$ -S relationships of the midlatitudes is quite consistent with the mixing between the two sources from high and low latitudes. To conclude, the strong  $\delta$ -S linearity ( $r \geq 0.95$ ) indicates a common origin of the water in this region, with decreasing salinity toward the north, according to increasing dilution of the NAD water with water from the SPG including MW from higher latitudes. Deviations to the regressions can be due to local freshwater inputs that are significantly  $^{18}\text{O}$ -enriched compared to the Y intercept (see the three local GNIP stations presented in Table 4: Altnabreac, Brest and Faro). Two samples at salinity  $\sim 35$  are above the main regression: they are located on the shelf Brest and must be influenced by local MW inputs (Figure 7).

### 5.2. The Tropical Atlantic Region

The Tropical Atlantic Ocean (red group in Figure 7) has been sampled mostly during April–May 2014 in the region of the Guinea Gulf (PIRATA FR24) with the other measurements collected during the summer 2016 further west (Cap San Lorenzo). Salinity ranges from 32.55 to 36.53,  $\delta^{18}\text{O}$  ranges from 0.55 to 1.06 $\text{‰}$ , and  $\delta\text{D}$  ranges from 5.24 to 7.95 $\text{‰}$ . The Y intercept is  $-3.04\text{‰}$  for  $\delta^{18}\text{O}$  and  $-9.71\text{‰}$  for  $\delta\text{D}$ . The correlation is relatively weak despite the high salinity range with  $r = 0.87$  for  $\delta^{18}\text{O}$  and  $r = 0.60$  for  $\delta\text{D}$ . The strong dispersion

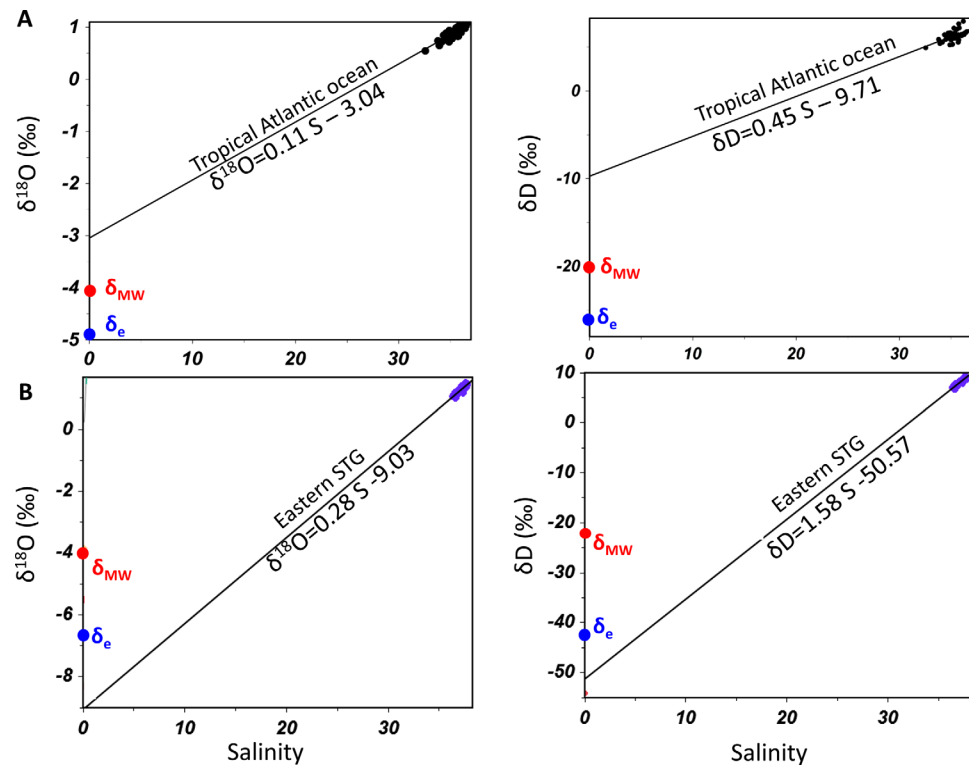


**Figure 8.** Overview of the  $\delta$ -S relationship extrapolated to zero salinity with indications of the  $\delta_e$  and  $\delta_{MW}$  values for (a) the tropical ocean and (b) the eastern STG. (left)  $\delta^{18}\text{O}$  and (right)  $\delta\text{D}$ .

could reflect the variability of freshwater sources at the surface, for example between local rainfall and river inputs.

In this region of high excess MW input, the Y intercept should be close to the isotopic composition of the freshwater sources. We collected rain samples from the ship to estimate the marine precipitation end-member (see Table 4 and Appendix A). Because the period of collection is short and does not represent an annual average, we also use the annual average weighted by the precipitation rate from two land GNIP stations at Douala (Cameroon) and Cotonou (Benin) (see Table 4). The two stations are dominated by humid air, limiting the reevaporation of rainwater, which is rather representative of marine conditions. We take the average of the GNIP stations (rather similar values) and the ship collection to represent the  $\delta_{MW}$  in this region ( $\delta_{MW}^{18}\text{O} = -3.91\text{‰}$  and  $\delta_{MW}\text{D} = -20.04\text{‰}$ ). Furthermore, we previously estimated an average value of  $\delta_e$  in the Guinea Gulf from the PIRATA cruise (see Table 3). Figure 8a shows the two end-members and the seawater  $\delta$ -S relationship over the tropical region, extrapolated to zero salinity. For both isotopes, the  $\delta_e$  is lower than  $\delta_{MW}$  and the Y intercept values for  $\delta^{18}\text{O}$ -S and  $\delta\text{D}$ -S are higher than  $\delta_{MW}$ . Therefore, from the mixed case in Figure 1c, we conclude that the  $\delta^{18}\text{O}$ -S and  $\delta\text{D}$ -S scatterplots indicate a major input of the near-equatorial enriched MW, with a minor contribution of evaporation.

### 5.3. The Subtropical Atlantic Ocean

The subtropical gyre is a region where E is usually much larger than MW. Thus, in contrast to the previous discussion, we expect that the Y intercept will be closer to  $\delta_e$  than to  $\delta_{MW}$ . We divide the STG in two parts, as the eastern and western part present different  $\delta$ -S relationships (Figure 7).

1. The eastern part. To estimate  $\delta_{MW}$  in the East subtropical region, we use two GNIP stations from the Azores Islands. The averaged rainwater isotopic compositions are very similar for the two stations (see Table 4). In addition, the measurements in the surface atmosphere in the eastern part of the STG suggest that  $\delta_e^{18}\text{O}$  ( $\delta_e\text{D}$ ) was  $\sim -8$  ( $-54$ )‰ during the winter 2015 (RARA 2) and  $\sim -5$  ( $-31$ )‰ during the summer 2012 (STRASSE) (Table 3). We calculate the average from the two seasons to estimate the average  $\delta_e$  in the region ( $\delta_e^{18}\text{O} = -6.7\text{‰}$  and  $\delta_e\text{D} = -42.5\text{‰}$ ). Figure 8b shows the two end-members and the

seawater  $\delta$ -S relationship over the eastern subtropical region. The  $\delta_e$  is lower than  $\delta_{MW}$ , as was also found in the tropical region but here the Y intercept values for  $\delta^{18}\text{O}$ -S and  $\delta\text{D}$ -S are lower than  $\delta_e$ . Therefore, from the mixed case in Figure 1c, we conclude that the  $\delta^{18}\text{O}$ -S and  $\delta\text{D}$ -S scatterplots indicate a main contribution of evaporation with a minor input of subtropical MW.

2. The western part. The water south of the STG is advected westward and skirts the Antilles archipelago within a northwestward current (see schematic circulation in Figure 2). Along this path, its salinity increases from  $\sim 35.8$  to  $\sim 36.6$  as a result of evaporation, and possibly entrainment of subsurface water. However, this water mass presents a different  $\delta$ -S relationship than the waters further east (see Figure 7). While the slopes are similar in the two regions, samples from the western part are shifted toward higher isotopic compositions for a given salinity. In the western part of the gyre and especially in the Gulf Stream area, MW inputs can be stronger and oceanic advection is more complex with additional water coming through the Gulf of Mexico and with a contribution from the SEC (see Figure 2). For these reasons, we are not able to provide a simple interpretation in the  $\delta$ -S scatterplots, as we did in the two previous regions by considering only two end-members. Nevertheless, we interpret the difference with the eastern part of the gyre, in part as the result of input of enriched tropical meteoric water from the South Equatorial Current and from the Amazon basin. Indeed, the GNIP data set shows that the average precipitation at Belem (Amazon estuary) is more enriched than the subtropical precipitation measured in the Eastern part of the gyre and at Bermuda (see Table 4). Furthermore, the 2016 seawater sampling a little bit north of the Amazon estuary (yellow group) is a good tracer of the Amazon freshwater source and the six samples with salinity ranging from 30.48 to 35.22 confirm the possibility of enriched tropical freshwater source affecting the western STG (higher Y intercept than in the eastern STG, Figure 7).
3. The STG of the South Atlantic. The few samples collected near  $10^\circ\text{S}$  and  $35^\circ\text{W}$  (orange group) represent the water of the South Atlantic STG along the Brazil current. They are close to the STG relationship of the Eastern North Atlantic, revealing similar processes in these two regions where  $E > P$ .

#### 5.4. Tropical Upwelling Influence

A few samples have been collected around Cabo Verde during the RARA cruise (Winter 2015) and off Senegal during the PIRATAFR24 cruise (Spring 2014) (magenta group in Figure 7). The salinity varies from 34.5 to 36.3 and the correlation with the isotopic composition is strong with  $r = 0.99$  for  $\delta^{18}\text{O}$  and  $r = 0.98$  for  $\delta\text{D}$ . These samples are located close to the Eastern STG samples (light green group), but do not follow the same regression (they are slightly below) and are fresher. The two southernmost samples ( $S = 35.62$ ,  $\delta^{18}\text{O} = 0.69\text{‰}$ ,  $\delta\text{D} = 4.27\text{‰}$  and  $S = 35.63$ ,  $\delta^{18}\text{O} = 0.73\text{‰}$ ,  $\delta\text{D} = 4.72\text{‰}$ ) located at ( $\sim 12$ – $14^\circ\text{N}$ ) could be influenced by upwelled water in the Senegal-Mauritania upwelling, thus probably indicative mostly of South Atlantic thermocline water having crossed the equatorial Atlantic. A little further north, the five samples located around Cabo Verde are not very different from the two previous samples and might also have a signature of upwelled water originating mostly from the southern hemisphere. The influence of these upwelled waters is also found in the highest-salinity area of the STG during the STRASSE cruise. In this area (square defined by  $26.5^\circ\text{N}$ ,  $25.5^\circ\text{N}$  and  $36^\circ\text{W}$ ,  $35^\circ\text{W}$ ), the salinity ranges from 37.50 to 37.75 and the isotopic dispersion is rather high (light green group in Figure 7). The spatial distribution (not shown here) reveals that most of the depleted samples for  $S \sim 37.65$  are located in the left and bottom corner of the study area. We know from salinity/temperature satellite measurements that this subarea was influenced by an eddy filament water coming from the south [Reverdin *et al.*, 2015]. The present investigation suggests that this filament could carry upwelled waters, which probably has a slightly more depleted  $\delta$  value (see magenta group). This is an example of how high-resolution isotope sampling can identify advection processes, even if salinity variations are small.

#### 5.5. The Mediterranean Sea

The western part of the Mediterranean Sea has been sampled during May and June 2016 (Figure 9). The surface salinity varies between 36.2 and 38.4. The two most depleted samples are influenced by freshwater inputs from the river Rhone. Two subsurface samples have been collected and correspond to the Levantine intermediate water (LIW) (370 m, 38.59) and to the bottom layer (2600 m, 38.49). These two highest saline samples, and in particular LIW, are influenced by the strongly evaporated surface water from the eastern Mediterranean Sea. We also add two samples near Gibraltar Strait with salinity  $S = 36.5$  to represent the source of fresher Atlantic waters. The  $\delta^{18}\text{O}$ -S and  $\delta\text{D}$ -S linear relationships are presented on the scatterplots of Figure 9. In order to characterize the evaporation process, we do not include the two samples strongly

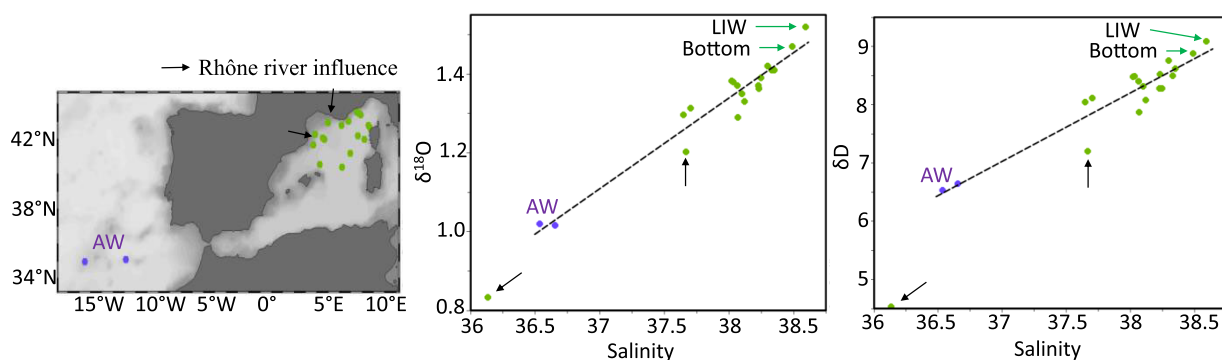


**Figure 9.** The  $\delta$ -S relationships in the Mediterranean Sea. The River Rhone influence is represented by a black arrow. The purple samples represent the fresh Atlantic Water source with salinity of  $\sim 36.5$ . The LIW sample is the most saline sample (370 m, 38.59). The bottom sample is the second most saline sample (2600 m, 38.49).

diluted with the waters from the River Rhone. The regressions are  $\delta^{18}\text{O} = 0.23 * S - 7.40$  ( $r = 0.97$ ) and  $\delta D = 1.17 * S - 36.44$  ( $r = 0.94$ ). No atmospheric measurements have been done during MOOSE-GE 2016 and we cannot estimate  $\delta_e$ . Delattre *et al.* [2015] measured the isotopic composition of the water vapor in the Rhone River delta (France) and record a strong variability of the isotopic composition of the ambient air in this coastal Mediterranean region. Nevertheless, the Y intercepts are higher and the slope are lower than those observed in the STG, suggesting a higher E:P ratio in the Mediterranean sea compared to the STG (see the  $\delta$ -S distributions in Figure 7).

## 6. Quantitative Estimates of E:MW Ratio

The previous sections showed the efficiency of the  $\delta$ -S relationship to capture the different hydrological conditions affecting the Atlantic Ocean and the Mediterranean Sea. In this section, we attempt to quantitatively estimate the ratio E:MW in different regions. For this purpose, we use the simple box model elaborated by Craig and Gordon [1965] (see equations in Appendix B). The model estimates the E:MW ratio as a function of the  $\delta$ -S relationship,  $\delta_e$  and  $\delta_{MW}$  and with the following assumptions: it neglects the mixing between different saline water masses, and it assumes that the salinity and the isotopic composition are in stationary state and that the net fluxes of water are balanced by the seawater supplied in the system. The model has already been applied in different regional basins [Ehnhalt, 1969; Andrié and Merlivat, 1989; Gat, 1996; Delaygue *et al.*, 2001; Conroy *et al.*, 2014]. Although these different studies show the role of the atmospheric forcing E and P on the  $\delta$ -S surface relationship, they also reveal important limitations, such as the difficulty to estimate  $\delta_e$  or multiple advection sources. Here we take advantage of a more complete data set to revisit this model in two contrasted regions where the assumptions can be tested: (i) the eastern part of the STG where E exceeds MW and (ii) the tropical Atlantic Ocean where MW exceeds E. The model, the assumptions and the sensitivity tests, are fully described in Appendix B, while the main results are resumed in the following.

In the subtropical region, the sensitivity of E:MW calculations to  $\delta_p$  values is relatively weak, while it is more sensitive to  $\delta_e$  value. Considering the average  $\delta_e$  over the eastern part of the STG (summer 2012 for STRASSE and winter 2015 for RARA 2), the model provides rather similar E:MW estimations for both isotopes, where E is approximately as the double of MW. In the tropical ocean where MW exceeds E, the method shows that the E:MW calculations are not very sensitive to  $\delta_e$  chosen (except when using the  $\delta_e$  average from RARA 2, but these values are not representative on the conditions usually encountered close to the equator), but are very sensitive to the  $\delta_p$  estimations. Considering the average  $\delta_p$  between the GNIP land stations (Douala and Cotonou) and the marine precipitation in the Guinea Gulf, calculation results in similar E:MW estimations for both isotopes, where MW is approximately twice as much as E.

To conclude, after careful considerations of the advection processes, this method gives consistent estimates of E:MW ratio. Moreover, reducing the uncertainties on  $\delta_p$  and  $\delta_e$  should provide precise estimations of the E:MW ratio at the ocean surface. We consider that this method is promising with the better simulation of the advective processes in oceanic models and with the increasing number of ship measurements that can be used to estimate  $\delta_e$ .

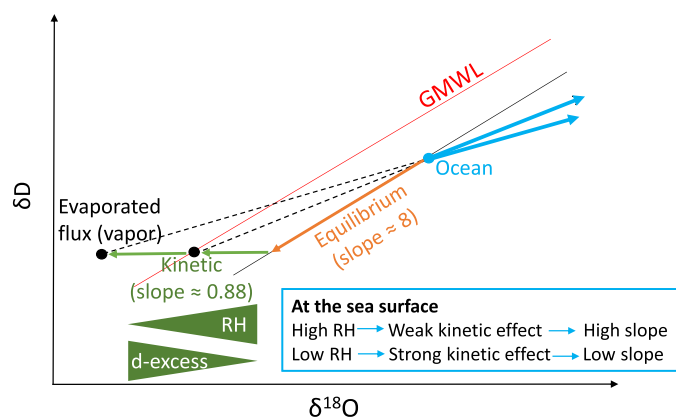


**Figure 10.** Evolution of the surface seawater in the  $\delta^{18}\text{O}$ - $\delta\text{D}$  space in a regime dominated by evaporation. The red line is the Global Meteoric Water Line ( $\delta\text{D} = 8 * \delta^{18}\text{O} + 10$ ). The evaporated flux can have different deuterium excess (d-excess), mainly as a function of the surface humidity, leading to different seawater  $\delta^{18}\text{O}$ - $\delta\text{D}$  relationship in basins of excess evaporation (low humidity leads to lower slopes). RH is relative humidity.

$\sim 8$ . However, during pure kinetic fractionation, the evaporated water vapor evolves along a slope of  $\sim 0.88$ , as the relative humidity varies. Therefore, deviations from the GMWL in the water vapor or rainwater are useful to investigate kinetic processes during reevaporation of rainwater [Dansgaard, 1964] or during evaporation at the ocean surface [e.g., Benetti et al., 2015]. To evaluate the contribution of kinetic processes, Dansgaard [1964] defined the deuterium excess (d-excess) as  $\delta\text{D} - 8 * \delta^{18}\text{O}$ . For example, low humidity at the sea surface produces a strong kinetic isotope effect, leading to high d-excess in the evaporated water vapor (Figure 10). Similar to rain and vapor, a  $\delta^{18}\text{O}$ - $\delta\text{D}$  relationship can be defined for surface seawater. From global surface samples (upper 250 m) the relation is  $\delta\text{D} = 7.37 * \delta^{18}\text{O} - 0.72$  [Rohling, 2007; Schmidt et al., 1999]. Here we investigate the regional variability of the seawater  $\delta^{18}\text{O}$ - $\delta\text{D}$  relationship over the surface Atlantic Ocean. We then interpret this variability considering the fractionation processes associated with evaporation and precipitation fluxes.

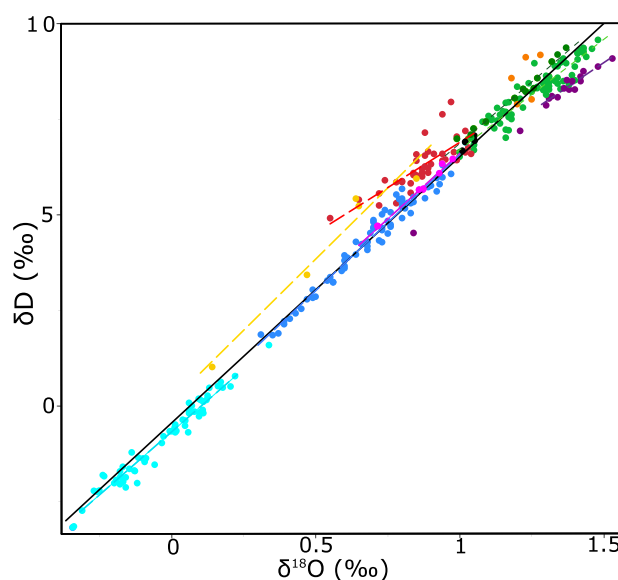


**Figure 11.** The  $\delta^{18}\text{O}$ - $\delta\text{D}$  relationship over the period 2010–2016. The black line is the linear regression from the 300 samples ( $\delta\text{D} = 6.96 * \delta^{18}\text{O} - 0.44$ ,  $r = 0.99$ ). The regional linear regressions are indicated with dashed lines and their equations are presented in Table 2.

## 7. The Seawater $\delta^{18}\text{O}$ - $\delta\text{D}$ Relationship

The  $\delta^{18}\text{O}$ - $\delta\text{D}$  relationship in the atmospheric portion of the hydrological cycle is mainly governed by the fractionation processes associated with evaporation and condensation. From global surveys of meteoric water (precipitation, continental runoff, and glacial meltwater), Craig [1961] defined a global meteoric water line (GMWL) as  $\delta\text{D} = 8 * \delta^{18}\text{O} + 10$ . At positive temperature, equilibrium fractionation of oxygen and hydrogen isotopes during condensation occurs proportionally with a factor of  $\sim 8$  (Figure 10). Accordingly, rain and residual water vapor evolve along a slope of

### 7.1. Variability at the Regional Scale

The same groups previously discussed are now identified in the  $\delta^{18}\text{O}$ - $\delta\text{D}$  diagram (Figure 11). The linear regression estimated from the  $\sim 300$  samples is  $\delta\text{D} = 6.96 * \delta^{18}\text{O} - 0.44$  with a very good correlation coefficient ( $r = 0.99$ ). Despite the diversity of the hydrological processes of the study area, it is clear that the  $\delta^{18}\text{O}$ - $\delta\text{D}$  relationship is more uniform compared to the  $S$ - $\delta^{18}\text{O}$  and  $S$ - $\delta\text{D}$  relationships. However, deviations from this slope can be detected at the regional scale. The two most northern groups (most depleted values), as well as the western part of the STG, are closest to the main regression line from the 300 samples. The strongest deviations are observed in the tropical ocean, the eastern part of the STG and the Mediterranean Sea. We found the lowest slope (4.73) in the tropical ocean and the second one in the Mediterranean Sea (5.07). The eastern part of

the STG has a slope of 5.80, with some samples of the eastern STG very close to the Mediterranean data distribution. Note that the few fresh samples from the Brazil Coast (five samples, yellow), strongly affected by the Amazon Basin MW inputs, also deviate from the main regression line.

## 7.2. Control of Atmospheric Water Fractionation Processes

In the following, we focus on the three main deviations from the main seawater  $\delta^{18}\text{O}$ - $\delta\text{D}$  relationship and explore the relation with the atmospheric fractionation processes. We consider first the tropical ocean, strongly affected by the MW inputs, as revealed by the  $\delta$ -S relationships. We now investigate how the low  $\delta^{18}\text{O}$ - $\delta\text{D}$  slope observed at the sea surface results from the  $\{\delta^{18}\text{O}$ - $\delta\text{D}\}$  pair distribution of the MW inputs. For this purpose, we simulate the slope in the  $\delta^{18}\text{O}$ - $\delta\text{D}$  diagram by diluting the saline end-member of the region with different sources of precipitation. The saline end-member is represented at salinity 36.3 and corresponds to the saltier water mass carried by the SEC and along the North East Brazilian coast, as well by the equatorial upwelling (see Figure B1b). The sources of precipitations we consider in the following discussion are (1) the average of 39 samples collected in May 2014 during the PIRATA cruise, (2) the annual average weighted by the precipitation rate from a GNIP station at Douala (Cameroon), (3) the annual average weighted by the precipitation rate from a GNIP station at Cotonou (Benin), (4) the annual average weighted by the precipitation rate from a GNIP station at Kano (Nigeria). The simulated  $\delta^{18}\text{O}$ - $\delta\text{D}$  slopes for each MW source are, respectively, (1) 5.80, (2) 4.99, (3) 4.81, and (4) 6.50. The slope simulated from the 39 rain samples collected from the ship is too high and suggests that these samples are not representative of the MW affecting the system. We also use one GNIP station at Kano, in the Sahel region, where reevaporation is expected due to the influence of surrounding dry air [Risi *et al.*, 2010], which could have induced a particularly low observed d-excess (6.55‰). This choice results in a too steep slope compared to what is observed. Then, we use the annual average weighted by the precipitation rate from two GNIP stations at Douala and Cotonou. The d-excess higher than 10 for the two stations reveal the weak impact of reevaporation of rainwater, confirming that both stations are rather representative of maritime conditions. The simulated slopes are lower and much closer to the observed slope. We conclude that low slope observed at the surface tropical Ocean can be reproduced with rainfall of high d-excess (close to  $\sim 11$ ‰) and not too much depleted precipitation. This implies that MW inputs over the tropical Ocean are mainly in equilibrium with the surrounding water vapor, with very little reevaporation. This is expected in this region dominated by humid lower troposphere air.

The two other strong deviations to the main  $\delta^{18}\text{O}$ - $\delta\text{D}$  relationship occurred in regions of excess evaporation. The two relationships are shifted to the right compared to the global seawater line, with lower slopes (5.07 for the Mediterranean Sea and 5.80 for the Eastern STG). In this region of excess evaporation, we theoretically expect to record an influence of the kinetic conditions during evaporation at the ocean surface on the  $\delta^{18}\text{O}$ - $\delta\text{D}$  seawater relationship. Figure 10 shows that the slope of the seawater data should become smaller when evaporation occurs at low sea surface humidity (stronger kinetic effect). Here we conclude that (i) the two lower slopes than the main  $\delta^{18}\text{O}$ - $\delta\text{D}$  relationship are due to the strong contribution of evaporation and (ii) the difference between the two slopes is due to the difference of humidity at the sea surface in the two regions. Indeed, the STG is dominated by the relatively humid oceanic trade winds while the Mediterranean Sea is dominated by drier continental air masses, especially in the eastern part [Romanou *et al.*, 2010], leading to a lower slope in the  $\delta^{18}\text{O}$ - $\delta\text{D}$  diagram. This result is consistent with the study of Delattre *et al.* [2015], in which 36 days of measurements reveal an average d-excess of 21.9‰ in air masses from the Mediterranean, largely higher than in the air masses from the North Atlantic (the average d-excess of the water vapor was  $10.3 \pm 2.9$ ‰ during the STRASSE cruise,  $11.2 \pm 1.4$ ‰ during the PIRATA cruise and  $11.6 \pm 5.1$ ‰ during the complete RARA cruise).

## 8. Conclusion and Outlook

This study contributes to the survey of the hydrological cycle variability [e.g., Durack, 2015] and improves our understanding of water stable isotopes in term of freshwater tracers. From 300 new samples, we characterized the surface  $\delta^{18}\text{O}$ -S,  $\delta\text{D}$ -S, and  $\delta^{18}\text{O}$ - $\delta\text{D}$  relationships over a large part of the Atlantic Ocean that will help to assess the oceanic modeling studies in which stable isotopes are implemented [e.g., LeGrande and Schmidt, 2006; Xu *et al.*, 2012]. The large spatial coverage indicates how the S- $\delta$  distributions can be used to identify different surface water masses and their horizontal advection (e.g., eddy features identified within

the STG or path of upwelled water from the Mauritania-Senegal upwelling). We also showed that the  $\delta$ -S distributions can provide information on the hydrological conditions, such as the dominant contribution of E or P, but only after carefully identifying the seawater sources, as well as the values characteristic of the evaporated and precipitated fluxes ( $\delta_e$  and  $\delta_p$ ). We showed that the different Y intercepts between the STG and the Mediterranean Sea corresponds to a higher E:P ratio in the Mediterranean Sea compared to the STG. One of the innovations of this study is to estimate  $\delta_e$  in different regions from 120 days of measurements of the ambient air above the sea surface. Clearly, this value cannot be considered as an average value of the  $\delta_e$  over the Atlantic Ocean and we encourage further measurements and comparisons with model simulations to obtain a more significant average, as well as to estimate its temporal and spatial variability. The data set underlines that the box model from *Craig and Gordon* [1965] should become an interesting framework to diagnose an average E:MW ratio over a region, with the recent implementation of the isotopes of seawater in models, the huge improvement of simulating the oceanic advection and the multiplicity of observations, both in seawater as in the water vapor above the ocean. Finally, we show the added value of the  $\delta^{18}\text{O}$ - $\delta\text{D}$  relationship compared to the more often used  $\delta$ -S relationship. First, the relatively high uniformity of the relationship, even in basins governed by different hydrological processes, is an advantage for past salinity reconstructions using the modern  $\delta^{18}\text{O}$ - $\delta\text{D}$  relationship of surface seawater [Fairbanks et al., 1997; van der Meer et al., 2007]. Then, in the tropical region where P exceeds E, the  $\delta^{18}\text{O}$ - $\delta\text{D}$  distribution can be used to identify the MW inputs from its kinetic signature. Evaluating  $\delta_p$  over the ocean remains an important concern as data at sea are too sparse to provide reasonable average estimates as illustrated for the PIRATA FR24 cruise. In the regions where E exceeds MW, the  $\delta^{18}\text{O}$ - $\delta\text{D}$  distributions were efficient to trace the humidity at the sea surface. This last property could be useful to trace paleo-humidity over the ocean, sea, or lake.

### Appendix A: Rain Measurements in the Guinea Gulf During the PIRATA FR24 Cruise

Table A1 presents the oxygen 18 and deuterium measurements of the 39 rain collected during the PIRATA FR24 cruise from 1 to 20 May 2014.

### Appendix B: Modeling Approach to Estimate E:MW

We use the simple box model elaborated by *Craig and Gordon* [1965] to calculate the E:MW ratio from the surface  $\delta$ -S relationship. This modeling approach results in equation (B1), which can be reformulated as a function of the slope of the  $\delta$ -S relationship to estimate the average E:MW of the basin (equation (B2)).

$$\delta = \delta_o + \left(\frac{S}{S_o} - 1\right) * \left( (\delta_o - \delta_e) + \frac{(\delta_e - \delta_{MW})}{\left(1 - \frac{E}{MW}\right)} \right), \tag{B1}$$

$$\frac{E}{MW} = \frac{\frac{d\delta}{dS} \cdot S_o - \delta_o + \delta_{MW}}{\frac{d\delta}{dS} \cdot S_o - \delta_o + \delta_e}, \tag{B2}$$

with  $S_o$  and  $\delta_o$  : salinity and isotopic composition of the seawater supplied the system,  $\delta_e$  and  $\delta_{MW}$  : average isotopic composition of the evaporated flux and MW, E and MW: average flux for evaporation and MW input,  $\frac{d\delta}{dS}$ : slope of the  $\delta$ -S relationship.

Because this model is based on a unique seawater source ( $S_o$  and  $\delta_o$ ), we only present E:MW calculations for the eastern STG and for the tropical Atlantic ocean, as the assumption is harder to set in the other regions of this study (see earlier sections and discussion on the advectons). The determination of  $S_o$  and  $\delta_o$  is discussed in the following.

In the eastern STG where E exceeds P, the oceanic sources are waters from the north carried by the NAC (black and blue samples in Figure B1a) and from the south or the east influenced by the upwelling (magenta samples). Because these different water masses have similar properties in the S- $\delta$  diagram, we can consider a single oceanic source defined by the black star in Figure B1a.

In the tropical Atlantic Ocean where P exceeds E, two main water masses are advected into the region (Figure B1b). One brings waters from the south, carried by the SEC and along the North East Brazilian coast, and

**Table A1.** Sea Rain Water Isotopic Data Collected During the PIRATA Cruise<sup>a</sup>

Time	Latitude	Longitude	Oxygen 18 (‰)	Deuterium (‰)	d-excess (‰)
4 May 14 5:24 A.M.	0.07	-9.91	-3.99	-21.79	10.13
4 May 14 2:14 P.M.	0.02	-9.63	-5.17	-27.49	13.88
4 May 14 2:19 P.M.			-5.36	-29.71	13.18
4 May 14 2:20 P.M.			-5.58	-31.71	12.95
4 May 14 2:24 P.M.			-5.65	-31.35	13.84
4 May 14 2:25 P.M.			-5.75	-34.01	12.02
4 May 14 2:29 P.M.			-5.58	-34.69	9.91
4 May 14 5:29 P.M.	0.00	-9.11	-6.58	-49.55	3.10
6 May 14 1:54 A.M.	0.00	-3.67	-3.85	-20.07	10.71
6 May 14 2:09 A.M.			-4.22	-25.29	8.47
6 May 14 2:14 A.M.			-4.61	-28.46	8.43
6 May 14 2:29 A.M.	0.00	-3.57	-5.21	-32.58	9.14
6 May 14 2:39 A.M.			-4.79	-27.25	11.05
6 May 14 2:49 A.M.			-4.14	-22.84	10.28
6 May 14 2:50 A.M.			-4.05	-22.90	9.53
6 May 14 3:25 A.M.	0.00	-3.40	-5.99	-40.70	7.23
6 May 14 7:54 A.M.	0.00	-2.62	-4.05	-22.25	10.16
6 May 14 8:00 A.M.			-5.27	-29.89	12.28
6 May 14 8:04 A.M.			-4.80	-27.11	11.33
6 May 14 8:05 A.M.			-4.38	-26.18	8.83
6 May 14 8:16 A.M.			-4.43	-24.57	10.87
6 May 14 8:21 A.M.			-4.61	-24.88	12.04
6 May 14 8:29 A.M.			-4.74	-26.77	11.18
6 May 14 7:54 P.M.	0.00	-2.58	-6.62	-37.68	15.26
6 May 14 8:15 P.M.			-9.74	-63.63	14.32
6 May 14 8:19 P.M.			-10.61	-72.17	12.70
8 May 14 6:39 P.M.	-0.57	0.93	-4.91	-28.27	11.05
8 May 14 6:53 P.M.			-6.89	-47.31	7.82
8 May 14 7:02 P.M.			-4.81	-29.17	9.28
10 May 14 6:13 A.M.	-5.00	8.12	-4.64	-24.86	12.25
10 May 14 6:20 A.M.			-2.03	-4.21	12.03
10 May 14 6:21 A.M.			-2.17	-8.60	8.80
10 May 14 1:30 P.M.	-5.00	9.46	-0.08	11.03	11.66
10 May 14 1:32 P.M.			-0.36	9.79	12.70
10 May 14 2:26 P.M.	-5.00	9.64	0.09	11.34	10.58
20 May 14 2:57 A.M.	4.67	-4.00	-5.01	-21.42	18.63
20 May 14 3:04 A.M.			-5.63	-25.08	19.93
20 May 14 3:24 A.M.			-5.93	-34.63	12.77
20 May 14 3:44 A.M.			-4.63	-24.36	12.66

<sup>a</sup>The 39 samples have been collected during the 20 days of the cruise.

the other brings water carried by the equatorial upwelling. All these waters originate from regions of excess evaporation and to simplify we identify a common saline end-member (S ~36.3) of the tropical δ-S relationship (black star in Figure B1b).

Table B1 presents E:MW calculations for each area, using the linear regressions presented in Table 2 and the oceanic source defined in Figure B1. In the subtropical region, this approach shows that the sensitivity of E:MW calculations to δ<sub>p</sub> uncertainties is relatively weak. The method using the average δ<sub>e</sub> over the eastern part of the SPG during Summer and Winter (STRASSE and RARA 2) provides reasonable E:MW estimates for both isotopes, where E is approximately twice as much as MW. If one uses only summer δ<sub>e</sub> value averaged over the STRASSE cruise, the estimations of E:MW are quite consistent for δ<sup>18</sup>O as for δD, but could be on the weak end, except for the calculation with the highest δ<sub>p</sub> value. On the other hand, using only the winter δ<sub>e</sub> value averaged over the RARA 2 period results in E:MW ratios different for the two isotopes, both being too large. In the near-equatorial ocean where MW exceeds E, the method shows that the E:MW calculations are not very sensitive to the δ<sub>e</sub> calculations (except when using the δ<sub>e</sub> average from RARA 2, but these values are not representative on the conditions usually encountered close to the equator). In the following, we use the average δ<sub>e</sub> in the Guinea Gulf (PIRATA FR24). The calculation using the average δ<sub>p</sub> (Douala, Cotonou, and Guinea Gulf) results in similar E:MW estimations for both isotopes, where P approximately doubles E. The similar E:MW estimated for the two isotopes is also found for other δ<sub>p</sub> and are very sensitive to the choice of the δ<sub>p</sub> value. Thus, while the values based on the average rain from the ship results in E:MW larger than 0.90, choosing the

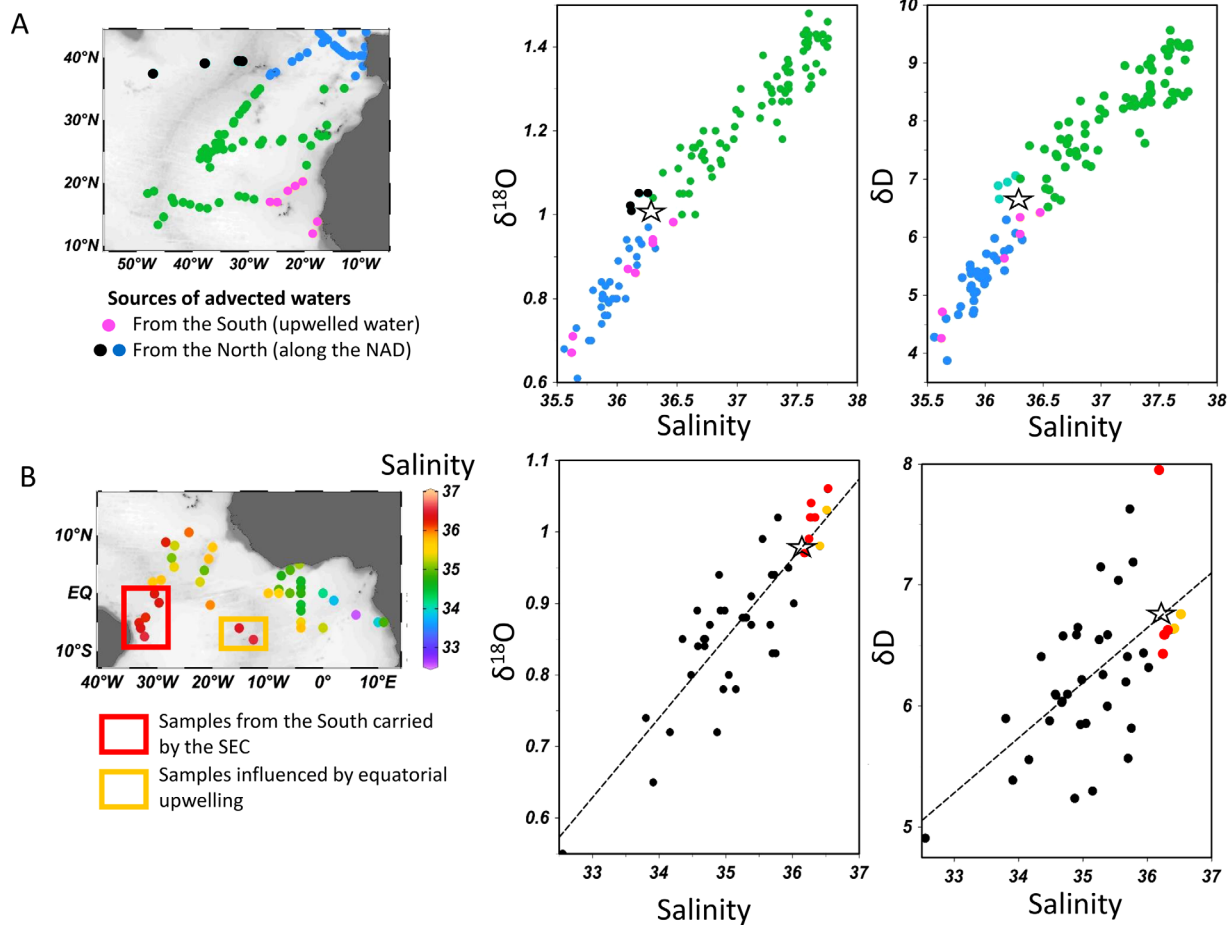


**Figure B1.** Two regions where the assumptions of the *Craig and Gordon's* [1965] box model can be tested. Multiple advected sources are highlighted for (a) the eastern part of the STG (black, blue, and magenta samples) and (b) the tropical Atlantic Ocean (mostly East) (yellow and red samples). The black star represents an assumed single seawater source for the region ( $S_w, \delta_w$ ). The seawater samples in each region are in (a) green and (b) black.

**Table B1.** Calculation of the E:W Ratio in Function of  $\delta_p$  and  $\delta_e$  for (A) the Eastern STG and (B) the Atlantic Tropical Ocean<sup>a</sup>

		$(\delta_p^{18}O, \delta_p D)$			
		-SD	Average	+SD	
(A) Case of the Eastern STG		(-4.82, -28.9)	(-3.92, -22)	(-3.02, -15.1)	
$(\delta_e^{18}O, \delta_e D)$	Summer	(-5.05, -31.02)	1.05/1.08	1.23/1.33	1.42/1.59
	Winter	(-8.30, -54.06)	3.18/7.03	3.74/8.69	4.30/10.34
	Average	(-6.68, -42.54)	1.58/1.85	1.85/2.31	2.13/2.75
		$(\delta_p^{18}O, \delta_p D)$			
		Guinea Gulf in May (Ship)	Annual Average (Douala and Cotonou)	Average	
(B) Case of the Atlantic Tropical Ocean		(-4.79, -26.96)	(-3.02, -13.10)	(-3.92, -20)	
$(\delta_e^{18}O, \delta_e D)$	Guinea Gulf	(-4.94, -27.27)	0.93/0.96	0.08/0.26	0.50/0.61
	Summer STG	(-5.05, -31.02)	0.88/0.82	0.07/0.22	0.48/0.52
	Winter STG	(-8.30, -54.06)	0.35/0.41	0.03/0.11	0.19/0.26

<sup>a</sup>(A) The intermediate  $\delta_p$  value is the annual average from the two land GNIP stations near the Azores Islands. The extrema values are estimated by adding or subtracting to the annual average one standard deviation of the seasonal variability. Only  $\delta_e$  values corresponding to the Eastern part of the STG are presented (the summer STRASSE cruise, the winter RARA 2 cruise, and the average of both cruises). (B) The  $\delta_p$  are estimated from the ship measurements in the Guinea Gulf during the May PIRATA cruise and from the two GNIP stations at Douala (Cameroon) and Cotonou (Benin). The last column is the average of the two values. The  $\delta_e$  has been measured in the tropical region only during the PIRATA cruise (Guinea Gulf). We also indicate the calculations with the  $\delta_e$  measured in the subtropical region, to evaluate the calculation sensitivity to  $\delta_e$ .

average from the two GNIP stations results in  $E:MW = 0.15$ . This large sensitivity to  $\delta_p$  results from  $\delta_p$  being close to  $\delta_e$ .

### Acknowledgments

The Picarro equipment was purchased with support from different French institutions, in particular by IPSL, LOCEAN, LMD, and LATMOS. Work during Strasse on R/V Thalassa and Pirata FR24 on R/V Suroit was supported by three LEFE/IMAGO INSU grants (Strasse, Strasse/SPURS, and PIRATA), with additional support for equipment from IPSL and from OSU Ecce Terra. The authors gratefully acknowledge the association "Les Amis du Jeudi et du Dimanche" for the measurements aboard the RARA AVIS. The authors thank the TOSCA-SMOS program whose founding was used for installing the SBE45 onboard the RaRa Avis Vessel. The Suratlant Project, as well as the data collection from the Toucan, Colibri and Cap San Lorenzo, are supported by SO SSS in France. Data collection onboard Ovide-2010 (doi:10.3334/CDIAC/OTG.CLIVAR\_OVIDE\_2010) and Ovide-2012 (doi:10.3334/CDIAC/OTG.CLIVAR\_OVIDE\_2012) cruises was supported by LEFE-INSU. We also acknowledge Philippe Poupon and Cedric Courson for the sampling aboard the sailing boat Fleur Austral, Tara Expéditions for the sampling aboard the sailing boat Tara, CSIC for the sampling aboard the Sarmiento de Gamboa during the Midas Cruise and MOOSE program (ALLENVI-INSU) for the sampling onboard R/V L'ATALANTE during the MOOSE-GE2016 cruise (doi:10.17600/16000700). The authors thank the National Power Company of Iceland Landsvirkjun for their contribution to this research. The data are shared with the free Global Seawater Oxygen-18 database [Schmidt et al., 1999].

### References

- Andrié, C., and L. Merlivat (1989), Contribution des données isotopiques de deutérium, oxygène-18, hélium-3 et tritium, à l'étude de la circulation de la Mer Rouge, *Oceanol. Acta*, 12(3), 165–174.
- Benetti, M., G. Reverdin, C. Pierre, L. Merlivat, C. Risi, H. C. Steen-Larsen, and F. Vimeux (2014), Deuterium excess in marine water vapor: Dependency on relative humidity and surface wind speed during evaporation, *J. Geophys. Res. Atmos.*, 119, 584–593, doi:10.1002/2013JD020535.
- Benetti, M., G. Aloisi, G. Reverdin, C. Risi, and G. Sèze (2015), Importance of boundary layer mixing for the isotopic composition of surface vapor over the subtropical North Atlantic Ocean, *J. Geophys. Res. Atmos.*, 120, 2190–2209, doi:10.1002/2014JD021947.
- Benetti, M., G. Reverdin, C. Pierre, S. Khatiwala, B. Tournadre, S. Olafsdottir, and A. Naamar (2016), Variability of sea ice melt and meteoric water input in the surface Labrador Current off Newfoundland, *J. Geophys. Res. Oceans*, 121, 2841–2855, doi:10.1002/2015JC011302.
- Benetti, M., G. Reverdin, C. Lique, I. Yashayaev, N. P. Holliday, E. Tynan, S. Torres-Valdes, P. Lherminier, P. Tréguer, and G. Sarthou (2017a), Composition of freshwater in the spring of 2014 on the southern Labrador shelf and slope, *J. Geophys. Res. Oceans*, 122, 1102–1121, doi:10.1002/2016JC012244.
- Benetti, M., et al. (2017b), Stable isotopes in the atmospheric marine boundary layer water vapour over the Atlantic Ocean, 2012–2015, *Sci. Data*, 4, Article 160128, doi:10.1038/sdata.2016.128.
- Benway, H. M., and A. C. Mix (2004), Oxygen isotopes, upper-ocean salinity, and precipitation sources in the eastern tropical Pacific, *Earth Planet. Sci. Lett.*, 224(3), 493–507.
- Bintanja, R., and F. M. Selten (2014), Future increases in Arctic precipitation linked to local evaporation and sea-ice retreat, *Nature*, 509(7501), 479–482, doi:10.1038/nature13259.
- Bourg, C., M. Stievenard, and J. Jouzel (2001), Hydrogen and oxygen isotopic composition of aqueous salt solutions by gas–water equilibration method, *Chem. Geol.*, 173(4), 331–337, doi:10.1016/S0009-2541(00)00282-5.
- Bower, A. S., B. Le Cann, T. Rossby, W. Zenk, J. Gould, K. Speer, P. L. Richardson, M. D. Prater, and H.-M. Zhang (2002), Directly measured mid-depth circulation in the northeastern North Atlantic Ocean, *Nature*, 419(6907), 603–607, doi:10.1038/nature01078.
- Conroy, J. L., K. M. Cobb, J. Lynch-Stieglitz, and P. J. Polissar (2014), Constraints on the salinity–oxygen isotope relationship in the central tropical Pacific Ocean, *Mar. Chem.*, 161, 26–33.
- Craig, H. (1961), Isotopic variations in meteoric waters, *Science*, 133(3465), 1702–1703.
- Craig, H., and L. I. Gordon (1965), Deuterium and Oxygen 18 Variations in the Ocean and the Marine Atmosphere, in *Proceedings of a Conference on Stable Isotopes in Oceanographic Studies and Paleotemperatures, Spoleto, July 26–27*, edited by E. Tongiorgi, pp. 9–130, Lab. of Geol. and Nucl. Sci., Pisa, Italy.
- Crosson, E. R., et al. (2002), Stable isotope ratios using cavity ring-down spectroscopy: Determination of  $^{13}C/^{12}C$  for carbon dioxide in human breath, *Anal. Chem.*, 74(9), 2003–2007.
- Dansgaard, W. (1954), The O18-abundance in fresh water, *Geochim. Cosmochim. Acta*, 6(5–6), 241–260, doi:10.1016/0016-7037(54)90003-4.
- Dansgaard, W. (1964), Stable isotopes in precipitation, *Tellus*, 16(4), 436–468, doi:10.1111/j.2153-3490.1964.tb00181.x.
- Delattre, H., C. Vallet-Coulomb, and C. Sonzogni (2015), Deuterium excess in the atmospheric water vapour of a Mediterranean coastal wetland: Regional vs. local signatures, *Atmos. Chem. Phys.*, 15(17), 10,167–10,181.
- Delaygue, G., E. Bard, C. Rollion, J. Jouzel, M. Stievenard, J.-C. Duplessy, and G. Ganssen (2001), Oxygen isotope/salinity relationship in the northern Indian Ocean, *J. Geophys. Res.*, 106(C3), 4565–4574, doi:10.1029/1999JC000061.
- Dodd, P. A., K. J. Heywood, M. P. Meredith, A. C. Naveira-Garabato, A. D. Marca, and K. K. Falkner (2009), Sources and fate of freshwater exported in the East Greenland Current, *Geophys. Res. Lett.*, 36, L19608, doi:10.1029/2009GL039663.
- Durack, P. (2015), Ocean salinity and the global water cycle, *Oceanography*, 28(1), 20–31, doi:10.5670/oceanog.2015.03.
- Durack, P. J., S. E. Wijffels, T. P. Boyer (2013), Long-term salinity changes and implications for the global water cycle, *Int. Geophys.*, 103, 727–757.
- Ehhalt, D. H. (1969), On the deuterium-salinity relationship in the Baltic Sea, *Tellus*, 21(3), 429–435.
- Epstein, S., and T. Mayeda (1953), Variation of O18 content of waters from natural sources, *Geochim. Cosmochim. Acta*, 4(5), 213–224.
- Fairbanks, R. G., M. N. Evans, J. L. Rubenstone, R. A. Mortlock, K. Broad, M. D. Moore, and C. D. Charles (1997), Evaluating climate indices and their geochemical proxies measured in corals, *Coral Reefs*, 16(5), 593–5100, doi:10.1007/s003380050245.
- Gaillard, F. (2015), ISAS-13 temperature and salinity gridded fields, SEANO, Issy-les-Moulineaux Cedex, France. [Available at <http://doi.org/10.17882/45945>]
- Gaillard, F., T. Reynaud, V. Thierry, N. Kolodziejczyk, and K. Von Schuckmann (2016), In situ–based reanalysis of the global ocean temperature and salinity with ISAS: Variability of the heat content and steric height, *J. Clim.*, 29(4), 1305–1323.
- Gat, J. R., A. Shemesh, E. Tziperman, A. Hecht, D. Georgopoulos, and O. Basturk (1996), The stable isotope composition of waters of the eastern Mediterranean Sea, *J. Geophys. Res.*, 101(C3), 6441–6451.
- Gordon, A. L., and C. F. Giulivi (2014), Ocean eddy freshwater flux convergence into the North Atlantic subtropics, *J. Geophys. Res. Oceans*, 119, 3327–3335, doi:10.1002/2013JC009596.
- Lécuyer, C., V. Gardien, T. Rigaudier, F. Fourel, F. Martineau, and A. Cros (2009), Oxygen isotope fractionation and equilibration kinetics between  $CO_2$  and  $H_2O$  as a function of salinity of aqueous solutions, *Chem. Geol.*, 264(1–4), 122–126, doi:10.1016/j.chemgeo.2009.02.017.
- LeGrande, A. N., and G. A. Schmidt (2006), Global gridded data set of the oxygen isotopic composition in seawater, *Geophys. Res. Lett.*, 33, L12604, doi:10.1029/2006GL026011.
- Majoube, M. (1971), Fractionnement en oxygène-18 et en deutérium entre l'eau et sa vapeur, *J. Chim. Phys.*, 68, 1423–1436.
- Merlivat, L., and J. Jouzel (1979), Global climatic interpretation of the deuterium-oxygen 18 relationship for precipitation, *J. Geophys. Res.*, 84(C8), 5029–5033, doi:10.1029/JC084iC08p05.
- Östlund, H. G., et al. (1987), *GEOSECS Atlantic, Pacific, and Indian Ocean Expeditions*, vol. 7, NSF, Washington, D. C. [Available at <http://epic.avi.de/34890/>]
- Peterson, B. J. (2002), Increasing river discharge to the Arctic Ocean, *Science*, 298(5601), 2171–2173, doi:10.1126/science.1077445.
- Reverdin, G., et al. (2015), Surface salinity in the North Atlantic subtropical gyre during the STRASSE/SPURS summer 2012 cruise, *Oceanography*, 28(1), 114–123.

- Risi, C., S. Bony, F. Vimeux, M. Chong, and L. Descroix (2010), Evolution of the stable water isotopic composition of the rain sampled along Sahelian squall lines, *Q. J. R. Meteorol. Soc.*, *136*(51), 227–242, doi:10.1002/qj.485.
- Rohling, E. J. (2007), Progress in paleosalinity: Overview and presentation of a new approach, *Paleoceanography*, *22*, PA3215, doi:10.1029/2007PA001437.
- Rohling, E. J., and G. R. Bigg (1998), Paleosalinity and  $\delta^{18}\text{O}$ : A critical assessment, *J. Geophys. Res.*, *103*(C1), 1307–1318.
- Romanou, A., G. Tselioudis, C. S. Zerefos, C.-A. Clayson, J. A. Curry, and A. Andersson (2010), Evaporation–precipitation variability over the Mediterranean and the Black Seas from satellite and reanalysis estimates, *J. Clim.*, *23*(19), 5268–5287, doi:10.1175/2010JCLI3525.1.
- Schmidt, G. A. (1999), Error analysis of paleosalinity calculations, *Paleoceanography*, *14*(3), 422–429, doi:10.1029/1999PA900008.
- Schmidt, G. A., G. R. Bigg, and E. J. Rohling (1999), Global Seawater Oxygen-18 Database, <https://data.giss.nasa.gov/o18data/>, NASA, Greenbelt, Md.
- Schmitt, R. W. (1995), The ocean component of the global water cycle, *Rev. Geophys.*, *33*(52), 1395–1409.
- Schmitt, R. W., P. S. Bogden, and C. E. Dorman (1989), Evaporation minus precipitation and density fluxes for the North Atlantic, *J. Phys. Oceanogr.*, *19*(9), 1208–1221, doi:10.1175/1520-0485(1989)019<1208:EMPADF>2.0.CO;2.
- Skrzypek, G., and D. Ford (2014), Stable isotope analysis of saline water samples on a cavity ring-down spectroscopy instrument, *Environ. Sci. and Technol.*, *48*(5), 2827–2834.
- Sofer, Z., and J. R. Gat (1972), Activities and concentrations of oxygen-18 in concentrated aqueous salt solutions: Analytical and geophysical implications, *Earth Planet. Sci. Lett.*, *15*(3), 232–238, doi:10.1016/0012-821X(72)90168-9.
- Sofer, Z., and J. R. Gat (1975), The isotope composition of evaporating brines: Effect of the isotopic activity ratio in saline solutions, *Earth Planet. Sci. Lett.*, *26*(2), 179–186, doi:10.1016/0012-821X(75)90085-0.
- Sutherland, D. A., R. S. Pickart, E. Peter Jones, K. Azetsu-Scott, A. Jane Eert, and J. Ólafsson (2009), Freshwater composition of the waters off southeast Greenland and their link to the Arctic Ocean, *J. Geophys. Res.*, *114*, C05020, doi:10.1029/2008JC004808.
- Terray, L., L. Corre, S. Cravatte, T. Delcroix, G. Reverdin, and A. Ribes (2012), Near-surface salinity as nature's rain gauge to detect human influence on the tropical water cycle, *J. Clim.*, *25*(3), 958–977.
- van der Meer, M. T. J., M. Baas, W. I. C. Rijpstra, G. Marino, E. J. Rohling, J. S. Sinninghe Damsté, and S. Schouten (2007), Hydrogen isotopic compositions of long-chain alkenones record freshwater flooding of the Eastern Mediterranean at the onset of sapropel deposition, *Earth Planet. Sci. Lett.*, *262*(3–4), 594–600, doi:10.1016/j.epsl.2007.08.014.
- Wüst, G., and A. Defant (1936), *Atlas zur Schichtung und Zirkulation des Atlantischen Ozeans: Schnitte und Karten von Temperatur, Salzgehalt und Dichte*, vol. 6, W. de Gruyter, Berlin.
- Xu, X., M. Werner, M. Butzin, and G. Lohmann (2012), Water isotope variations in the global ocean model MPI-OM, *Geosci. Model Dev.*, *5*(3), 809–818.
- Yu, L. (2007), Global variations in oceanic evaporation (1958–2005): The role of the changing wind speed, *J. Clim.*, *20*(21), 5376–5390, doi:10.1175/2007JCLI1714.1.